DISSERTATIONS IN
FORESTRY AND
NATURAL SCIENCES

Rinat Ismagilov

Formation of carbon nano- and micro-structures by chemical vapor deposition

Publications of the University of Eastern Finland
Dissertations in Forestry and Natural Sciences No 127

UNIVERSITY OF
EASTERN FINLAND

RINAT ISMAGILOV

Formation of carbon nano- and micro-structures by chemical vapor deposition

Publications of the University of Eastern Finland
Dissertations in Forestry and Natural Science No 127

Academic Dissertation
To be presented by permission of the Faculty of Science and Forestry for public examination in the Auditorium M100 in Metria Building at the University of Eastern Finland, Joensuu, on October, 24, 2013, at 12 o'clock noon

Department of Physics and Mathematics

Kopijyvä OY
Joensuu, 2013
Editors: Prof. Pertti Pasanen,
Prof. Pekka Kilpeläinen, Prof. Kai Peiponen, Prof. Matti Vornanen

Distribution:
Eastern Finland University Library / Sales of publications
P.O.Box 107, FI-80101 Joensuu, Finland
tel. +358-50-3058396
http://www.uef.fi/kirjasto
ISBN: 978-952-61-1264-0 (nid.)
ISBN: 978-952-61-1265-7 (PDF)
ISSNL: 1798-5668
ISSN: 1798-5668
ISSN: 1798-5676 (PDF)

Author's address:

University of Eastern Finland
Department of Physics and Mathematics
P.O.Box 111
80101 JOENSUU
FINLAND
email: rinat.ismagilov@gmail.com

Supervisors:

Professor Alexander N. Obraztsov, Ph.D.
Department of Physics and Mathematics
University of Eastern Finland
P.O.Box 111
FI-80101 JOENSUU
FINLAND
email: alexander.obraztsov@uef.fi

Reviewers:

Professor Andrzej Huczko, Ph.D.
Faculty of Chemistry
University of Warsaw
PL-02-093 WARSAW
POLAND
email: ahuczko@chem.uw.edu.pl

Professor Catherine Journet-Gautier, Ph.D.
Laboratoire des
Multimatériaux et Interfaces
Université Lyon 1
FR-69622 LYON
FRANCE
email:
catherine.journet-gautier@univ-lyon1.fr

Opponent:

Professor Esko Kauppinen, Ph.D.
Department of Applied Physics
Aalto University
P.O. Box 15100
Puumiehenkuja 2
FI-00076, ESPOO
FINLAND
email: esko.kauppinen@hut.fi

ABSTRACT

This thesis reports on the experimental investigations directed for production and characterization of thin film carbon materials. The nano- and micro-structured carbons were obtained in this study with use of plasma enhanced chemical vapor deposition include: single and few-layered graphene; polycrystalline diamonds films consisting of nano- and micrometer sized grain; composites of diamond and graphitic carbons; textured polycrystalline diamond films, composed of needle-like crystallites. The composition and structural properties were obtained with use of Raman spectroscopy, electron microscopy and diffraction. The experimental analysis was performed to establish interrelation between parameters of the deposition process and characteristics of the obtained films. In-situ monitoring of the plasma activated carbonaceous gas mixture has been performed with use of optical emission spectroscopy. The empirical models and mechanism were proposed to explain experimental observations and predict possible ways for optimization process parameters and achieve pre-requested material properties.

Keywords: plasma-enhanced chemical vapor deposition, carbon, nanocarbon, single and polycrystalline diamond, diamond tips, graphite, few-layered graphene, thermal oxidation, optical emission spectroscopy, Raman, SEM, TEM

Universal Decimal Classification: 538.958, 543.573, 620.187, 620.183.24

PACS Classification: 81.05.U-, 81.05.ug, 81.05.uj, 81.05.ue, 81.05.uf, 81.07.Bc, 61.50.Ks, 64.70.Hz, 81.10.Jt, 61.66.-f, 81.15.Gh, 82.80.Gk, 82.33.Xj, 52.70.-m, 81.16.Pr, 64.75.Lm, 32.30.-r, 78.30.Hv, 68.37.Hk, 68.37.Lp

Preface

This Thesis would not exist if I had not received support from so many people.

I would like to take this opportunity to thank some of them:
Above all, I am profoundly indebted to my supervisor Professor Alexander N. Obraztsov for his valuable guidance, fundamental insight, who was very generous with his time and knowledge;
Professor Yuri Svirko for freely sharing his wide expertise;
Professor Markku Kuittinen, Professor Pasi Vahima, Professor Timo Jääskeläinen for providing me the opportunity to realize my research project in the University of Eastern Finland;
I am grateful to the official reviewers of this thesis, Professor Andrzej Huczko and Professor Catherine Journet-Gautier, for their professional review and encouraging comments.
My special thanks are for Aleksey Zolotukhin, Pertti Pääkkönen, Tommi Itkonen, Olga Svirko, Victor Prokofiev, Unto Pieviläinen who gave me extended guidance, instructions and help in everyday work with equipments;
I am very grateful to Hannele Karppinen, Katri Mustonen, Noora Heikkilä, Timo Vahimaa for great administrative and IT support;
I would express also my thanks to "UEF Nanocarbon team" including Dmitry Lyashenko, Petr Obraztsov, Mikhail Petrov, Tommi Kaplas, Viatcheslav Vanyukov, Feruza Tuyakova for their great support and creating extremely favorable conditions for scientific work;
Many thanks to all co-authors and co-workers, including Jarkko Mutanen, Hemmo Tuovinen, Martti Silvennoinen, Anastasia V. Tyurnina, Andrei L. Chuvilin for helpful discussions;
My wife, parents, brothers for their love and encouragements, for always being by my side no matter what.

LIST OF ORIGINAL PUBLICATIONS

This thesis consists of the present review of the author's work in the field of plasma enhanced chemical vapor deposition and the following selection of the author's publications:

I **R.R. Ismagilov**, P.V. Shvets, A.A. Zolotukhin, A.N. Obraztsov, "Optical characterization of plasma chemical vapor deposition of nanocarbon film materials", Journal of Nanoelectronics and Optoelectronics 4, 243–246 (2009).
II A. Zolotukhin, P.G. Kopylov, **R.R. Ismagilov**, A.N. Obraztsov. "Thermal oxidation of CVD diamond", Diamond and Related Materials 19, 1007-1011 (2010).
III A.V. Tyurnina, **R.R. Ismagilov**, A.V. Chuvilin, A.N. Obraztsov. "Topology peculiarities of graphite films of nanometer thickness", Physica Status Solidi B 247, 3010-3013 (2010).
IV A.N. Obraztsov, P.G. Kopylov, B.A. Loginov, M.A. Dolganov, **R.R. Ismagilov**, N.V. Savenko "Single crystal diamond tips for scanning probe microscopy", Review of Scientific Instruments 81, 013703 (2010).
V A.A. Zolotukhin, **R.R. Ismagilov**, M.A. Dolganov, A.N. Obraztsov, "Morphology and Raman spectra peculiarities of chemical vapor deposition diamond films", Journal of Nanoelectronics and Optoelectronics 7, 22–28 (2012).
VI **R.R. Ismagilov**, A.A. Zolotukhin, P.V. Shvets, A.N. Obraztsov, "Spatially resolved in situ diagnostics for plasma-enhanced CVD carbon film growth", Journal of Nanoelectronics and Optoelectronics 7, 90–94 (2012).

Throughout the overview, these papers will be referred to by Roman numerals. The original articles have been reproduced with permission of the copyright holders.

In addition the author has the following peer-reviewed journal articles related to the research work:
1. T. Kaplas, R. Ismagilov, A. Obraztsov, Yu. Svirko "Characterization of nanographite by specular gloss measurements", Journal of Nanoelectronics and Optoelectronics 7, 54–59 (2012)
2. R.R. Ismagilov, P.V. Shvets P.V., A.Yu. Kharin, A.N. Obraztsov "Noncatalytic synthesis of carbon nanotubes by chemical vapor deposition", Crystallography Reports 56, 310-314 (2011)
3. P.G. Kopylov, B.A. Loginov, R.R. Ismagilov, A.N. Obraztsov "Single-crystal diamond probes for atomic-force microscopy", Instruments and Experimental Techniques 53, 613-619 (2010)
4. S.A. Lyashenko, A.P. Volkov, R.R. Ismagilov, A.N. Obraztsov "Field electron emission from nanodiamond", Technical Physics Letters 35, 249-252 (2009)
5. R. R. Ismagilov, A. P. Volkov, P. V. Shvets, and A. N. Obraztsov "Physical and Chemical Processes in Gas-Discharge Plasma During the Deposition of Nanocarbon Films", Protection of Metals and Physical Chemistry of Surfaces, 45, 652–655 (2009).

AUTHOR'S CONTRIBUTION

The publications selected in this dissertation are original research papers on plasma enhanced chemical vapor deposition of carbon materials.
In the papers **I, VI** the author personally planned and performed experiments on carbon film deposition, measurements of optical emission of plasma. The author has contributed in the interpretation of the experimental results and in writing of all these papers. In the papers **II – V** the author partially carried out experimental works on fabrication and characterization of the carbon structures.
In all papers the cooperation with the co-authors has been significant.

Contents

1 Introduction

Intensive researches in nanoscale materials have been inspired by discovery of new forms of materials exhibiting unique properties that they may possess due to their low dimensionality [1]. Special interest to carbon materials in view of the nanoscience and nanotechnology is because of extraordinary ability of this chemical element to combine with itself and other chemical elements in different ways (chemical versatility), which is not only the basis of life and of organic chemistry, but also gives rise to a rich diversity of structural forms of solid materials composed only by carbon, including in micro- and nano-scale ranges.

Thin-film materials, consisted of covalently bonded carbon atoms, have been of considerable interest from both fundamental and applied perspectives in the last 50 years since the chemical vapor deposition (CVD) of diamond was developed, followed by discovery of fullerenes, carbon nanotubes, and graphene [2–6]. A large majority of graphitic and other carbon products are now synthetic and these products are continuously being improved and upgraded, although natural graphite and diamond still remains the material of choice in a few cases [7]. Despite carbon materials production by CVD are used since 80th of previous century, full understanding of the physics and chemistry behind formation of the condensed matter from activated gas environment is still challenging. It is caused by high complexity of the phenomena occurring in the activated gaseous environment. Nowadays, in order to get CVD insights, scientists and engineers invent different experimental systems, develop theoretical frameworks, and start to increasingly use computer simulations, which have been evolved as an essential part of scientific research, complementing theory and experiment [8–10]. In this thesis, some progress is brought to the experimental part of this field of research. This thesis provides demonstrations of production of different carbon structures together with the analysis of processes occurring in plasma environment during their formation by chemical vapor deposition. We have studied the chemical vapor deposition in wide range of process parameters and reveal some peculiarities in formation of carbonaceous solids from methane-hydrogen gas mixture activated by a direct current (DC) discharge.

The subsequent chapter 2 of this thesis briefly discusses the structure, molecule peculiarities, fabrication, characterization, and potential application of carbon materials. Chapter 3 dedicated to low-pressure plasma, which was used in all experimental works. In chapter 3, original CVD equipment is introduced. This chapter gives an overview of found CVD process parameters providing reproducible deposition of different types of uniform thin film carbon materials. Chapter 4 discusses the CVD of single and few-layered graphene on Ni and Si

substrates, while chapter 5 discusses the diamond films. In chapter 6 some concluding remarks and outlooks are made.

2 Carbon materials (short survey)

Carbon is a truly remarkable element which participates in very important and very different chemicals. The condensed forms of elemental carbon exist in several allotropes. Pure elemental carbon is found mainly in nature as coal or as natural graphite, and much less abundantly as diamond [11]. Moreover, the solid carbons may be readily obtained from the pyrolysis of various hydrocarbons from methane and acetylene to such as resins and pitches, and can be deposited from the vapor phase by cracking hydrocarbon rich gases [12]. In its various allotropic forms carbon has quite remarkable properties [13–20]. Some of these allotropic forms and their properties (mainly structural and morphological) are considered in this chapter.

2.1 STRUCTURE AND BONDING IN CARBON MATERIALS

Carbon allotropes (or polymorphs) consist of the same single element, but their atomic arrangements are quite different [12,7]. The atomic configurations determined by interatomic bondings formed between the carbon atoms during material formation process. In ground state electronic configuration of carbon atoms is $(ls^2)(2s^2 2p_x 2p_y)$ which allows formation of sp^3, sp^2 and sp^1 orbitals as a result of promotion and hybridization (fuller accounts can be found in many standard chemistry textbook, e.g. [21]).

There are four equivalent sp^3 hybrid orbitals that are tetrahedrally oriented about the carbon atom and can form four equivalent tetrahedral σ bonds by overlapping of the orbitals of neighboring atoms. An example of such atomic configuration is the molecule ethane, C_2H_6, where a Csp^3-Csp^3 (or C-C) σ bond is formed between two C atoms by overlapping of sp^3 orbitals, and three Csp^3-H1s σ bonds are formed on each C atom (see **Fig.1a**).

Another type of hybridization of the valence electrons in the carbon atom can occur to form three sp^2 hybrid orbitals leaving one unhybridized 2p orbital. These three sp^2 orbitals are equivalent, coplanar and oriented at 120° to each other and form σ bonds by overlapping with the orbitals of neighboring atoms, as, for example, in the molecule ethene C_2H_4 (see **Fig.1b**). The remaining p orbital on each C atom forms a π bond by overlapping of the p orbital from the neighboring C atom; the bonds formed between two C atoms in this way are represented as Csp^2=Csp^2 (or C=C).

In the third type of hybridization of the valence electrons of carbon, two linear 2sp orbitals are formed leaving two unhybridized 2p orbitals. Linear σ bonds are formed by overlapping of the sp hybrid orbitals with orbitals of neighboring atoms,

as, for example, in the molecule ethyne (acetylene) C_2H_2 (see **Fig.1c**). The unhybridized p orbitals of the carbon atoms overlap to form two π bonds; the bonds formed between two C atoms in this way are represented as Csp≡Csp (or C≡C). We shall limit our discussion to primarily the first two types of atomic bonding and consider only graphite- and diamond-like structures, correspondingly.

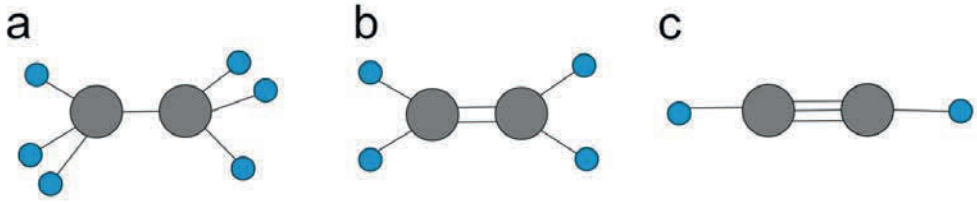

Fig.1. *Some molecules with different C-C bonds: (a) ethane; (b) ethene; (c) ethyne.*

The diamond as well as graphite crystals were the subjects for application of X-ray diffraction at early stage of development of this technique (see, e.g. [22]). Diamond is most frequently found in a cubic crystal lattice form in which each carbon atom is linked to four other carbon atoms by sp^3 σ bonds in a tetrahedral array (**Fig.2**). The diamond crystal structure is Zinc-blende type and the C-C bond length is 154 pm. Diamond also exists in hexagonal form (Lonsdaleite) with a Wurtzite crystal structure and a C-C bond length of 152 pm. The crystal density of both types of diamond is 3.52 $g \cdot cm^{-3}$. Notably, the shearing action during cutting might transform some of the cubic diamond to hexagonal diamond [23].

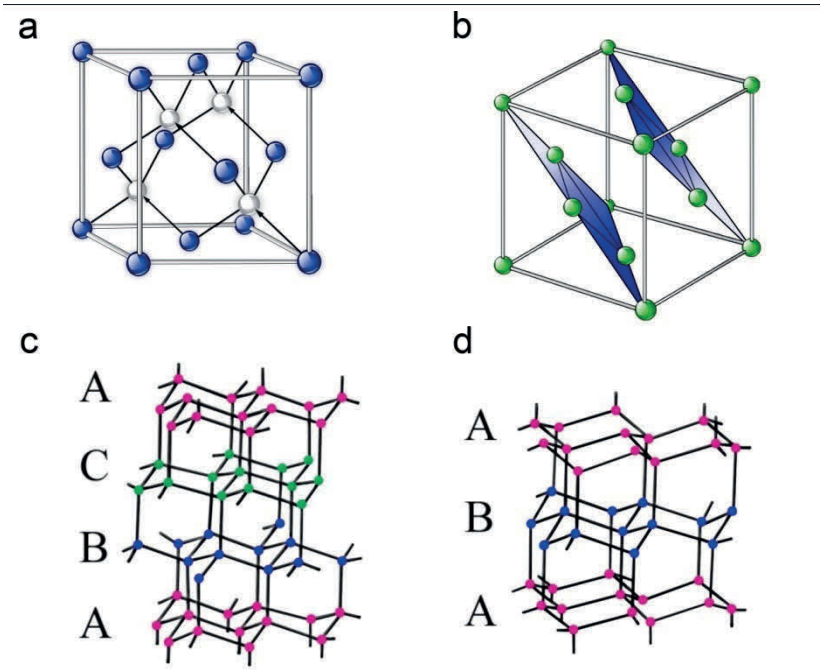

Fig.2. *Diamond Cubic and Lonsdaleite structures. (a) diamond as face-centered cubic crystal (fcc); (b) layered representation of fcc; (c) and (d) – layers sequence for Cubic diamond and Lonsdaleite*

Graphite also may exist in few forms from which the most frequently one is hexagonal graphite. The basic element of the crystal structure of graphite is graphene, i.e. carbon atoms, arranged into plane structure with one-atom thick honeycomb lattice, joined together by strongly localized sp^2 σ bonding and delocalized π bonding. The commonest crystal form of graphite is hexagonal and consists of a stack of layer planes in the stacking sequence ABABAB … (**Fig.3**).

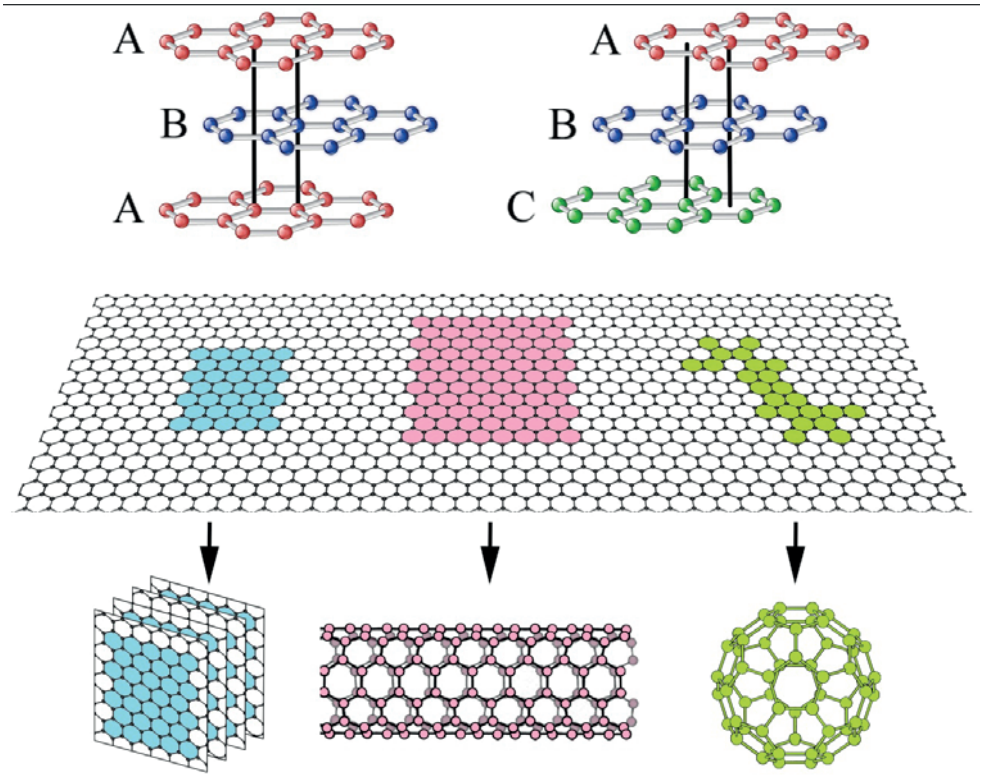

Fig.3. *Hexagonal and rhombohedral structures of graphite(top); Graphite, nanotube and fullerene as derivatives of graphene (bottom)*

The rhombohedral form of graphite with a stacking sequence ABCABC... is an alternative component of well-crystallized graphites while other forms with more complicated (rarely) or disordered stacking are also possible. The proportion of rhombohedral graphite can be increased by deformation processes, such as grinding [12]. Conversely, the proportion of rhombohedral graphite can be reduced by high temperature heat-treatment, showing that the hexagonal form is more thermodynamically stable. For both forms of graphite the in-plane C-C distance is 142 pm, i.e., intermediate between Csp^3-Csp^3 and Csp^2=Csp^2 bond lengths, 153 and 132 pm respectively. The density of both forms of graphite is 2.26 $g \cdot cm^{-3}$. [12]

It should be noted, that the monoatomic carbon layer - graphene is a structural basic element also for carbon nanotubes [24,2,4], fullerenes [25,3,26,27] (see **Fig.3.**), nanocones and many other nanostructured carbon materials [28,29]. Some experimental results on carbon nanotube and nanoscrolls (see article 2, 4 listed above) were obtained with use of the same CVD techniques. However nanotubes, fullerenes and other similar derivatives from graphene carbon materials are out of the scope of this thesis. A detailed description of these materials may be found in e.g. [30–32].

2.2 FABRICATION OF CARBON MATERIALS

Many new carbon materials demonstrating unique characteristics have been obtained in the last decades.

A common characteristic of graphite- and diamond-like carbon materials, whatever their origin or processing, is that they may be derived from organic precursors: molded graphite from petroleum coke and coal-tar, pyrolytic graphite from methane and other gaseous hydrocarbons, vitreous carbon and fibers from polymers, carbon black from natural gas, charcoal from wood, coal from plants, etc. [33]. These organic precursors must be carbonized and more often graphitized, in order to form carbon and graphite materials. The *carbonization* process, also known as pyrolysis, can be defined as the step in which the organic precursor is transformed into a material that contains substantially only carbon atoms. The precursor is heated slowly in a reducing or inert environment, over a range of temperature that varies with the nature of the particular precursor and may extend to 1300°C. The organic material is decomposed into a carbon residue and volatile compounds diffuse out to the atmosphere. Another common step after carbonization is *graphitization*, which implies heating treatment at temperatures often in excess of 2500°C [34,35]. Graphitization can be defined as the transformation of a disordered turbostratic graphitic material into a well-ordered graphitic structure. The graphitization mechanism includes: (a) removal of most defects within each graphite layer plane as well as between the planes, (b) gradual shifting and growth of the crystallites, (c) removal of cross-linking bonds, (d) evolution of the ABAB stacking sequence, and (e) shifting of carbon rings or single atoms to fill vacancies and eliminate dislocations [7]. This fabrication technique (carbonization and graphitization) allow obtaining parts of considerable size, weighing several hundred kilograms, such as the industrial electrodes, which are industrially manufactured in large quantities.

Graphitic products obtained from organic binder by subsequent carbonization and graphitization usually divided to two distinctive groups of carbon materials: the molded carbons and the vitreous carbons. The former are derived from precursors that graphitize readily, while latter does not graphitize readily and has characteristics and properties that are essentially isotropic. The difference between materials of these two classes stems from different precursor materials.

Another emerging technique of carbon materials fabrication is *chemical vapor deposition* (CVD) in which condensed carbon produced by the entirely different processes. The main difference of CVD from usual carbonization and graphitization is that the CVD based on a gaseous precursor instead of a solid or liquid. CVD is a powerful and versatile technique that has been used for carbon thin-film deposition and surface treatment since the early 1960s [36]. CVD-produced carbon materials span a continuum in grain sizes, morphologies, defect structures and concentrations, and properties, from high quality, nearly perfect single crystals to polycrystalline materials where the grain size can vary continuously from barely displaying evidence of crystallinity to mm-sized grains [37].

Nowadays, CVD from a gas mixture containing the carbonaceous components activated by the electrical discharges of different types become a usual way of fabrication different kinds of carbon materials covering the substrates, including various nanoscale particles and films (carbon nanotubes [38–42], nanocones [43,44], few-layered graphene [45–48], nanodiamond [37,49,50] and other materials from carbon "family" [28]). Despite CVD of carbon materials has been used since last century, full understanding of physics and chemistry behind solid formation from activated gas environment are still challenging. It caused by high complexity of the phenomenon, which requires simultaneously consideration of several processes including mass transport (flows of different reactive species), heat transport (through radiations, convection, and conduction), activated gas and surface chemistry (considering hundreds of reactions, see e.g. [51–54]), etc.

2.3 CHARACTERIZATION OF CVD CARBON

Since Raman spectroscopy is a fast, informative and non-destructive technique for carbon material characterization [55,56], it was the first and main method applied for sample identification in our work. Nowadays, Raman spectroscopy is the most widely used characterization technique in analyzing carbon films, because of its ability to distinguish the vibrational modes (phonons) of sp^3 and sp^2 bonding configuration in carbon materials [57].

Ideal single-crystal graphite exhibits a Raman first-order spectrum of a single line at 1580cm^{-1} [58]. The "graphite" line (G line) shifts down to lower frequencies and broadens [11] and another Raman line, the D line, begins to grow at a value 1350cm^{-1}, when small microcrystallites form, or when bond-angle disorder is introduced [59]. The G peak is assigned to photon scattering via interaction with graphitic optic zone center phonons (which can be estimated to honeycomb arrangement of carbon atoms with C-C bonding in sp^2 hybridization [17]). The D peak arises from the scattering by disorder-activated optical zone edge phonons. 2D-peak in the second-order Raman scattering originates from double resonance mechanism and its position is about 2700cm^{-1} [60]. This peak is suited for characterization of few-layered graphene. The intensity of 2D-peak in relation to G-peak and its shape give direct evidence to the number of layers in examined few-layered graphene [61]. For monolayer graphene 2D feature is a single Lorentzian line with an intensity of about 2-4 times of G band [62].

The ratio of the Raman scattering efficiency for graphite and diamond is about 50:1 for "green" excitation lasers [23]. Raman spectroscopy, therefore, is a very effective tool for characterization the quality of CVD diamond films and identification of small amounts of graphite in diamond [11]. For diamond, the first-order Raman band appears as a single sharp line at about 1332 cm^{-1} [23]. In case of nanodiamond, the Raman spectrum contains also two peaks centered at 1140 and 1470 cm^{-1}, which assigned to transpolyacetylene segments at grain boundaries and surfaces [63]. Besides identification of carbon materials, Raman spectroscopy

allows estimation additional internal properties of carbon films (e.g. using pressure dependence curve [64], it is possible to interpret the small wavenumber shifts as internal stresses; temperature sensitivity of G peak allows extraction the value of thermal conductivity [65]).

The interpretation of Raman spectra is fairly straightforward for characterization of mono phases. It gets complicated when the system contains mixed phases (sp^3 and sp^2) due to the large difference in scattering cross-sections for visible excitation wavelengths [66]. This problem somewhat rectified by using UV source since the photon energy closer to the band gap of sp^3-bonded carbon. However, *quantitative* estimation of sp^3 bonding in mixed phases is still ambiguous. Thus, care should be taken when using the Raman spectra for more than *qualitative* analysis in mixed-phases of carbon materials [67].

The combination of analytical methods (e.g., Raman spectroscopy) and electron microscopy allow getting detailed insights into the characteristics of crystalline materials. A great advantage of the transmission electron microscopy is in the capability to observe, by adjusting the electron lenses, both electron microscope images (information in real space) and diffraction patterns (information in reciprocal space) [68,69]. The transformation from the real space to the reciprocal space is mathematically given by the Fourier transform. While interpretation of images obtained by an electron microscope is intuitively simple, the understanding of diffraction patterns usually requires additional skills [70].

If electron beam covers many disordered crystallites, the electron diffraction pattern consists of characteristic rings. This situation arose in case of polycrystalline and amorphous carbon materials (e.g. see electron diffraction patterns for nanodiamonds in [71], bunch of nanotubes in [72]). If electron beam interact with a single crystal, the electron diffraction pattern has characteristic array of spots (e.g. see electron diffraction patterns for few-layered graphene in [73], a single crystal of diamond in [74]). Notably, the recently developed microdiffraction methods, where incident electrons are converged on a specimen, can now be used to get diffraction pattern from an area only a few nm in diameter.

In present study the structure peculiarities of carbon materials was analyzed by Raman spectroscopy and electron diffraction technique, while morphology was investigated by optical and scanning electron microscopy. The usage of the described techniques (Raman spectroscopy and electron microscopy) with accompanying comments will be discussed in following chapters.

2.4 PROPERTIES AND POTENTIAL APPLICATIONS OF CARBON MATERIALS

If one virtually chooses any characteristic property of a material (structural, electrical or optical), the value associated with carbon materials will almost always represent an extreme position among all materials considered for that properties. Nowadays, carbon material deposition techniques enable the exploitation more and

more properties combinations of single-phase and composite carbon materials (e.g., combination of optical activity and biocompatible of the diamond-like materials extend the range of their usage in bio-applications [75]). Listing all of the possible permutations of combinations would result in a small book itself [11,76]. Several potential applications that can be applied to materials obtained in a scope of this thesis work are listed below.

Exceptional mechanical, thermal, optical, and electronic properties make diamond very attractive for numerous applications. The superlative hardness of diamond renders it ideal for cutting applications [77], while its optical transmissivity renders it ideal for an extremely broad spectrum of signals, which might be useful, for example, for optical quantum computing [78–82]. The diamond, possessing wide-bandgap (5,5eV), potentially enables devices that are beyond the scope of current systems in terms of operating frequency, power handling capacity, operating voltage, and operating environment [76]. Moreover, combination of extremely low coefficient of friction with hardness of CVD diamond, render it ideal for use in oilless bearings [83]. The desirable chemical, biological, and physical properties of nanodiamond make them wholesome in biomedical applications, including purification, sensing, imaging, and drug delivery [50].

Graphene, few-layered graphene, flaky nanographite posses a unique combination of extraordinary mechanical, electrical, thermal and optical properties [84,16,5,85]. The giant optical rectification in such materials renders them ideal for fast-response photodetector and THz generator applications [86,87]. The canvas-like structure and impenetrability makes few-layered graphene to be ideal for many applications where nanoscale materials should be isolated from the environment or biological tissue [88]. The chemical inertness, sustainability to ion bombardment, high electrical conductivity make carbon materials suitable for application in field (cold) electron emission to create intense beams of electrons in the vacuum electronic devices [89]. Notably, besides applied interest, carbon materials are in focus of several fundamental studies. Few-layered graphene, for example, is an unique laboratory for investigations of nature phenomenon caused by lowering material dimensionality (see e.g. the probable mechanisms behind the drastic alteration of a material's intrinsic ability to conduct heat as its dimensionality changes from two to three dimensions in [90]).

3 Physics and chemistry of plasma

This chapter dedicated to the current research in the field of chemically reactive plasmas. The following discussion of papers dealing with low-temperature plasma-enhanced chemical vapor deposition of carbon materials is not meant to be exhaustive, but it is believed to be representative of current work in this field. The structure of chapter is composed in such a way in order to "point" the place of author's contributions (articles **I, VI**) in a "big picture" of this research field.

3.1 INTRODUCTION

Low temperature plasma is an ionized gas with free electrons and free positive and negative ions showing collective behavior. As whole, it exhibits quasi-neutral behavior with the same number of positive ions and negative ions and electrons. Plasma is usually formed by applying constant or alternating electric or electromagnetic fields to a low pressure gas mixture. Plasma properties (electron and ion densities, electron energy distribution function, plasma composition, electron and gas temperature, etc) result from the equilibrium between power dissipation in heating of electrons, generation of plasma species in electron collisions and the losses due to recombination in the gas phase or at the wall [91]. The electrons with high average energy of several electron volts control ionization, dissociation and excitation of molecules and atoms, hence, extend the role of their temperature, which become the driving force in chemical vapor deposition processes. Heavy particles (atoms, radicals, ions) can stay at moderate temperatures slightly above room temperature (room temperature to a few hundreds of Kelvins) [92]. The high kinetic energy of electrons makes plasmas nonselective with a high fragmentation degree, which makes it difficult to predict the results of plasma-chemical processes. [91]

In low-temperature plasmas, a precursor gas is ionized and dissociated, and radicals as well as ions impinging onto the substrate lead to carbon film growth. This enables the preparation of films with superior material properties and allows access to a wide range of carbon nano- and microstructures. However, despite this great importance in many applications, the underlying growth mechanisms during chemical vapor deposition process are poorly understood. This is due to the complexity of the growth process: the spectrum of species arriving at the surface can be very diverse, consisting of ions, radicals and neutrals as well as electrons and high-energy photons. All these species can participate in film formation and promote mutual strengthening or weakening of their contributions in the growth process [93].

The existence of the variety species arriving at the surface, their chemical and physical properties (concentration, transport energies, the excitation rate of inner states and etc.) usually determined through complementary experimental and theoretical investigations, conducted for sufficiently large plasma area [94,51,52,54,95]. The difficulties in theoretical, compute-based investigation usually strengthen because of luck or inaccessibility special tabulated data (e.g. the scattering cross sections) for exotic species at abnormal conditions (e.g. see [96]), because of mathematical difficulties due to the solving of system of coupled non-linear partial differential equations, a large number of coexisting reaction channels (see e.g. [52,97], where considered 81 reactions in methane/hydrogen plasma).

An additional factor contributing to plasma physics and chemistry complexity is the number of system variables used for processes optimization, including equipment variables (reactor size and configuration, materials of construction, method and amount of power applied); gas variables (pressure, flow, gas composition and ratios); and substrate variables (substrate temperature, material, crystallinity, and location in reactor). Often, small changes in a single parameter can result in large changes in the overall process chemistry. In some systems, the balance between etching and deposition is so sensitive to these parameters that controlling the outcome is challenging and miscalculations can result in significant waste. [98]

Experimentally, bulk plasma processes usually investigated using optical technique applied to different plasma areas [98], while the interaction of active species with surfaces can be studied in particle beam experiments. *In the latter case*, with the exact knowledge of the surface structure and of the angular and energy distribution for the incoming and outgoing species, very detailed conclusions on the interaction mechanisms can be drawn. One example is the interaction of fluorine with silicon as the elementary step in silicon etching [99]. However, in many growth plasmas the dominant precursors for film growth are larger radicals such as CH_3, C_2, etc. The preparation of a well defined particle beam of these species, which is essential for this type of study, can be difficult. Therefore, only little is known on the microscopic surface mechanisms of these precursors [93]. It should be noted, there are exist several works related to the investigation of the surface interaction with an effusive molecular beam consisting of virtually all species present in the plasma, including the species of interest (see e.g. [100]). *In the former case*, an array of techniques can be applied to the examination of plasma processes, including optical emission spectroscopy (OES), optical absorption spectroscopy, laser-induced fluorescence, cavity ringdown absorption spectroscopy, Fourier transform infrared spectroscopy [98]. In works **I, VI** OES technique has been used to reveal some plasma features during carbon deposition. *Generally*, this technique is based on collection and investigation photons emitted by plasma, by activated gas-phase species. Gas-phase species are promoted to excited electronic states by collisions with energetic electrons and relaxation is accompanied by emission of a photon. Information about these photons can be gathered by OES technique. OES is usually used for a qualitative determination of the composition

via monitoring the presence or absence of the particular spectral lines. *Particularly*, OES measures the emission from excited states of species, which are normally formed by electron impact excitation of the corresponding ground state species (the spatial distribution of particularly excited atoms proportional to the atoms at ground state, electron density, and electron temperature distributions) [51]. The emission intensities are thus closely linked with the properties of electrons in the plasma. As a result, OES measurements can provide valuable information about electron energy distribution function, electron temperature and concentration, and their variation with changes in process condition [101,102]. OES is recognized as a valuable technique for monitoring and optimizing plasma processes because of its high sensitivity and flexibility in operation.

In order to rationalize bewildering array of plasma observations the sequence of main growth species and chemical reactions is usually postulated [103]. Special attention in the field of carbon material deposition is paid to different active species, including C, C_2, CH, CH_2, CH_3, C_2H, C_2H_2, H, H_2 [104–111]. We limit discussion as well as our description of experimental observations with reactive dicarbon C_2 species. It is widely accepted that graphite or amorphous carbon is closely linked to the presence of carbon dimers C_2 in the plasma, due to frequent observations of correlation of deposits structure with the species in the plasma [15]. Moreover, these correlation strengthened by the fact that C_2 is one of the carbon species resulting from the sublimation of graphite. While the influence of C_2 on deposition of graphite-like materials seems to be clear, understanding the impact of carbon dimers on the growth of nano- or diamond-like carbon (DLC) is blurred. There is no common view on the C_2 influence during DLC growth. It is widely accepted that C_2 is a dominant growth species during the (110) surface formation of diamond [15,112]. However, several works suggest that C_2 does not play a major role in the growth of nanocrystalline diamond [115,111].

There is an extensive scientific and industrial interest in hydrocarbon plasma chemistry and physics since it plays an important role in creation of fascinating materials for many applications. However, despite this interest, the hydrocarbon physic-chemistry and carbon-based film growth mechanisms are still not well understood. The primary reason is the ability of carbon to form double and triple bonds leading to a large family of radicals, molecules and ions coexisting together in the gas phase. Almost any combination of hydrogen and carbon atoms can exist in the form of several isomers, which can make very stable organic compounds. The densities of these species have to be measured, spatially and temporally resolved in the best case, to be able to understand the plasma physic-chemistry involved. This is putting high demands on the diagnostic tools and requires combined experimental and theoretical modeling efforts. The articles **I, VI** represent an experimental contribution to the "body of knowledge" of plasma deposition science. Experimental investigation's details of plasma-enhanced CVD system and OES are described below.

3.2 EXPERIMENTAL

The methane-hydrogen gas mixture activated by a DC discharge has been the main investigated plasma object in this work. Moreover, this plasma was used for production different types of carbon materials (see also chapters 4, 5). **Fig.4.** shows a schema of the deposition setup with anode (bottom electrode) and cathode (upper electrode) connected with a current source power supply. The electrodes situated inside a reactor chamber are cooled by chilling water. The total gas pressure, methane concentration and substrate temperature, as well as the discharge voltage and current, were varied to obtain the film-like materials with different carbon phase compositions. A special attention was paid to provide the discharge stabilization by using control circuits preventing the discharge arcing. The structure and composition of the obtained carbon film materials were characterized qualitatively by a Raman spectroscopy and an electron microscopy. The Raman measurements were performed using Jobin-Yvon U 1000 instrument with the excitation by Ar-ion laser at 514.5 nm in a backscattering geometry.

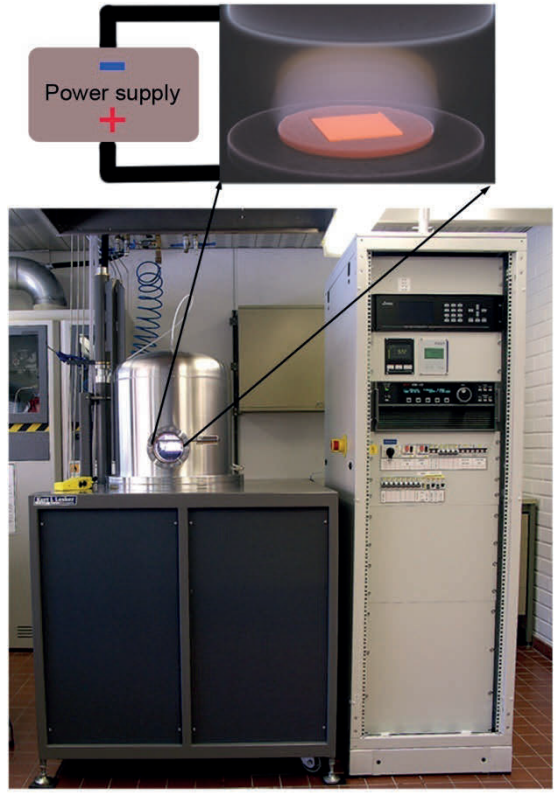

Fig.4. *Photo and scheme of CVD equipment*

Fig.5a shows a schematic diagram of the OES experimental setup. Two viewports with the fused quartz windows in the walls of the plasma-enhanced CVD reactor chamber (see **Fig.5**) provide in-situ optical observation of the plasma with a necked eye or with a CCD camera. An optical pyrometer was used for measurements of the substrate temperature during the deposition process. Imaging of the plasma ball on a screen (1:1 scale) located outside the reactor chamber was made using a quartz objective. The screen was fixed on a table movable in two directions (vertical and horizontal) with micrometer accuracy. A throughout hole in the screen allows collecting the portion of the light generated by plasma onto an entrance of an optical fibre connected with a spectrometer (HR4000-UV-NIR, Ocean). The acquisition and analysis of the digital information from the CCD camera and spectrometer was made on a personal computer (PC in **Fig.5a**). **Fig.5b** shows an example of a typical rectangular area of the DC plasma where the spatial distributions of the gas discharge plasma parameters were determined by using a scanning movement of the screen with the optical fiber. Additionally to that, an estimation of the time evolution of the spatial distribution of C_2 dimers was performed using the CCD camera with an optical interference filter (a maximum filter transmission was at 514.5 nm, FWHH 10 nm) in front of the entrance objective.

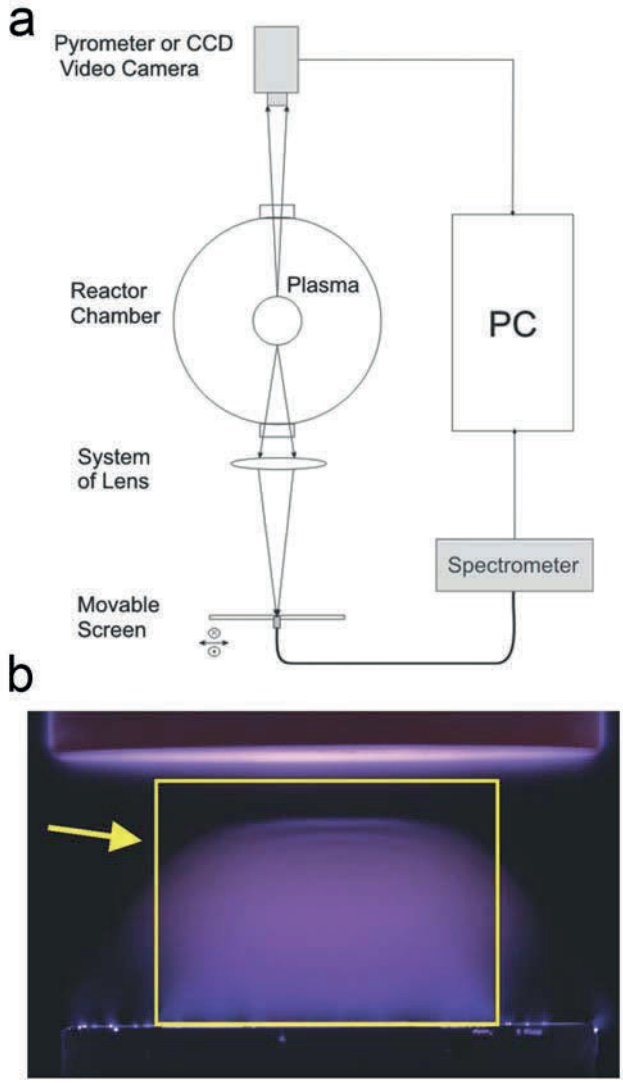

Fig.5. *(**a**) A schematic top view of the OES and the temperature measurement apparatus attached to PECVD chamber. (**b**) A photograph of the DC discharge and the rectangle area being interesting for OES pointed with an arrow*

3.3 RESULT AND DISCUSSION

A comparative analysis of the plasma parameters along with the results of Raman and electron microscopy measurements allow us to reveal the regimes at which the polycrystalline diamond, nanocrystalline diamond, graphite-like

nanostructured carbon films can be deposited on flat substrates due to interaction with the methane-hydrogen gas mixture activated by the DC discharge.

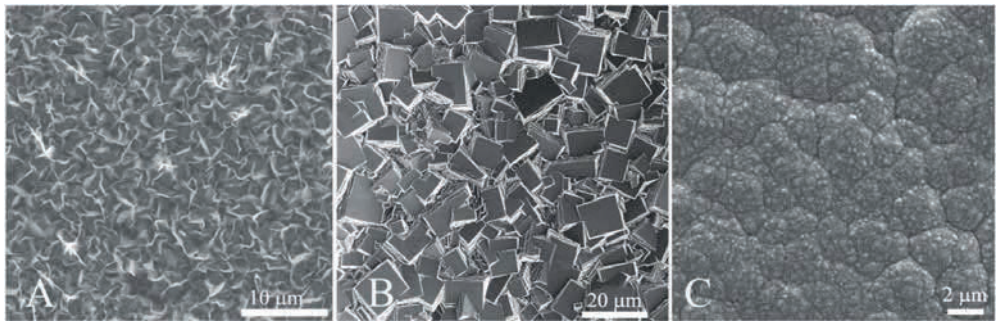

Fig. 6. *The SEM images of typical CVD films: (**A**) Nanocrystalline graphite; (**B**) poly-crystalline diamond; (**C**) nanocrystalline diamond*

Fig.6 shows the scanning electron micrographs (SEM) of the most typical carbon film materials. Raman spectra of the films are presented in **Fig.7**. These SEM images and Raman spectra correspond to a nanocrystalline graphite material (A), a polycrystalline diamond film (B), a nanocrystalline diamond film (C). Raman lines meaning was described earlier (see paragraph 2.3).

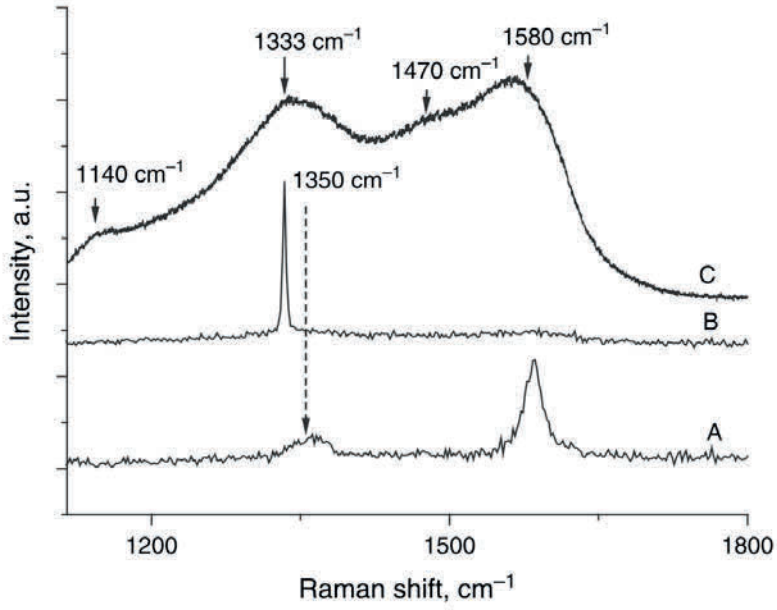

Fig. 7. *The Raman spectra of typical CVD films: (**A**) nano-crystalline graphite; (**B**) poly-crystalline diamond; (**C**) nano-crystalline diamond*

The CVD process parameters being the most appropriate for a reproducible deposition of different carbon films are summarized in **Table I**. These correlations represents small part of optimization results, which also include relation characteristics of the deposits with substrate material and temperature, flow rates, DC voltage, configuration of plasma area and etc. Generally all results consistent and complement the common condensation tendency of carbon materials from gas phase (see e.g. [116]). Some of particularly interesting findings will be discussed below (see next chapters).

Table 1. *The experimental parameters for carbon films deposition in DC-discharge plasma*

Type of CVD film material	**Methane concentration (%)**	**Total gas pressure (Torr)**
Diamond	0.5 – 2	60 – 90
Nanocrystalline diamond	2 – 5	60 – 100
Graphite-like	5 -10	60 – 100
Soot	Over 15	50 – 100

The range of conducted OES investigation of plasma was limited by plasmas which achieve the non-equilibrium but stationary state and keep it for a long time. Moreover, additional limitation of the conducted number of OES experiments was caused by time consuming spatial scanning procedure, which implies the manual movement of screen and analyzing data from single spatial point (manual scanning).

As an example, a typical optical emission spectrum obtained for the plasma glowing in the hydrogen-methane gas mixture with 3.7% methane at a scanning point near 2.5 mm above the substrate surface in its central region is presented in **Fig.8**. The Swan system with the Q(0, 0) band head at 516.5 nm as the most intense emission band attributed to C_2 and two atomic hydrogen emission lines at 656 nm (H_α) and at 486 nm (H_β) of the Balmer transition series are clearly seen. During OES inspection the main attention was paid to these revealed emission lines.

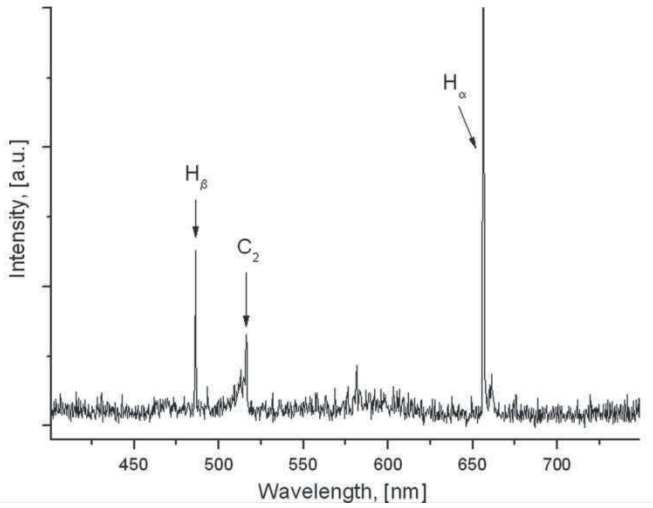

Fig. 8. *The optical emission spectrum for a hydrogen-methane gas mixture with 3.7% methane, near 2.5 mm above the substrate surface in its central region*

The Balmer transition series were used for electron temperature estimation, while tracing emission C_2 lines were used for evaluation the relative spatial distribution of C_2 active plasma species in plasma.

We have used the relative intensities of the lines emitted by excited hydrogen atoms in order to determine the excitation temperature (T_{exc}) which can give a first estimation of the electron temperature in low pressure CH_4/H_2 plasma under investigation. In obtaining the values of T_{exc} , we have assumed that the upper energy levels of the selected atomic transitions are in local thermodynamic equilibrium (LTE), that is, the population density of such levels follows the Boltzmann law. The latter allows us to use the conventional Boltzmann plot technique to determine T_{exc} by using the expression [102]

$$\ln\left(\frac{I_{ij}\lambda_{ij}}{g_i A_{ij}}\right) = -\frac{E_i}{kT_{exc}} + C \qquad (1)$$

where I_{ij} is the relative intensity of the emission line between the energy levels i and j, λ_{ij} its wavelength, g_i is the degeneracy or statistical weight of the emitting upper level i of the studied transition, and A_{ij} is the transition probability for spontaneous radiative emission from the level i to the lower level j. Finally, E_i is the excitation energy of level i, k is the Boltzmann constant and C is constant. It is important to stress, that determined temperature T_{exc} [by using (1)] equals to electron temperature of plasma in case of the LTE condition. This case is realized if the population of the upper excited levels is determined by collisions with electron only. A necessary condition for the existence of the LTE is that the electron density N_e has to be more than ~10^{14} cm^{-3} (the lower limit of electron density obtained supposing the electron temperature kT_e is equal to *ca.* 1 eV). In our experiments (as

it was done in work [117]) the electron density could be estimated from the equation $N_e=j/(e\upsilon_e)$, where j is the electric current density, e is the electron charge, υ_e is the drift electron velocity. The value of these parameters (j, e, υ_e) were taken from [118]. The estimation of the electron density for conditions corresponding to used CVD process gives $N_e \approx 1.5\times10^{12}$ cm^{-3}. Hence, in our case, a local thermodynamic equilibrium does not really exist, and for this reason the electron temperature value shown below may be considered only as a rough estimation. However, it makes sense as an illustration of a general regularity in the temperature distribution in a plasma volume and its dependence on the conditions of the gas discharge.

The absolute densities of the active species in plasma environment are usually estimated by using different absorption techniques [119–122]. However in some cases the rough concentration estimation can be obtained via OES measurements. The *absolute* concentration and distribution of C_2 species in our plasma is not known but it is possible to estimate a relative density regularity, supposing that the emission intensity of the $d^3\Pi \rightarrow a^3\Pi(0, 0)$ vibrational band of the C_2 Swan system in methane hydrogen plasma correlates linearly with the absolute C_2 concentration. This assumption can be supported by inspections conducted for similar plasma. E.g. in [123,124] revealed linear concentration correlation of C_2 dimers obtained via absorption measurements with the emission intensity of the main the $d^3\Pi \rightarrow a^3\Pi(0, 0)$ vibrational band of the C_2 Swan system. However, it should be noted, that it is desirable to conduct additional absorption experiments and time consuming computer simulations to verify OES results. Such experiments are planned and their preliminary results are not included to this thesis.

By performing the spectral measurements at different points inside the rectangular plasma area of interest we estimate the spatial distributions of the electron temperature and emission intensity of the line corresponding to C_2 species. As a rule, the electron temperature profile appeared to be alike the profile of the emission intensity spatial distribution of the line corresponding to C_2 species (**Fig.9**). The spatial distribution maximum is near the surfaces of the electrodes and other maximum is localized around the central axis at the distances ranging from about 5 to 25 mm from the substrate (anode). As expected, the relative emission intensity of the line corresponding to C_2 species much higher in case of graphite-like material deposition than diamond-like materials growth (see **VI)**. The appearance of this carbonaceous species in the gas mixture near a substrate surface correlates with the formation of graphite-like films. This correlation of the nature of the deposits with the species in the plasma led to conclusion that graphite-like carbon is closely linked to the presence of carbon dimers C_2 in the plasma. Moreover, in some deposition conditions dust particles have been found in the plasma volume (see **I)**. Such experimental results impose additional requirements for theoretical modeling of plasma, which should include physics and chemistry of dust particles too.

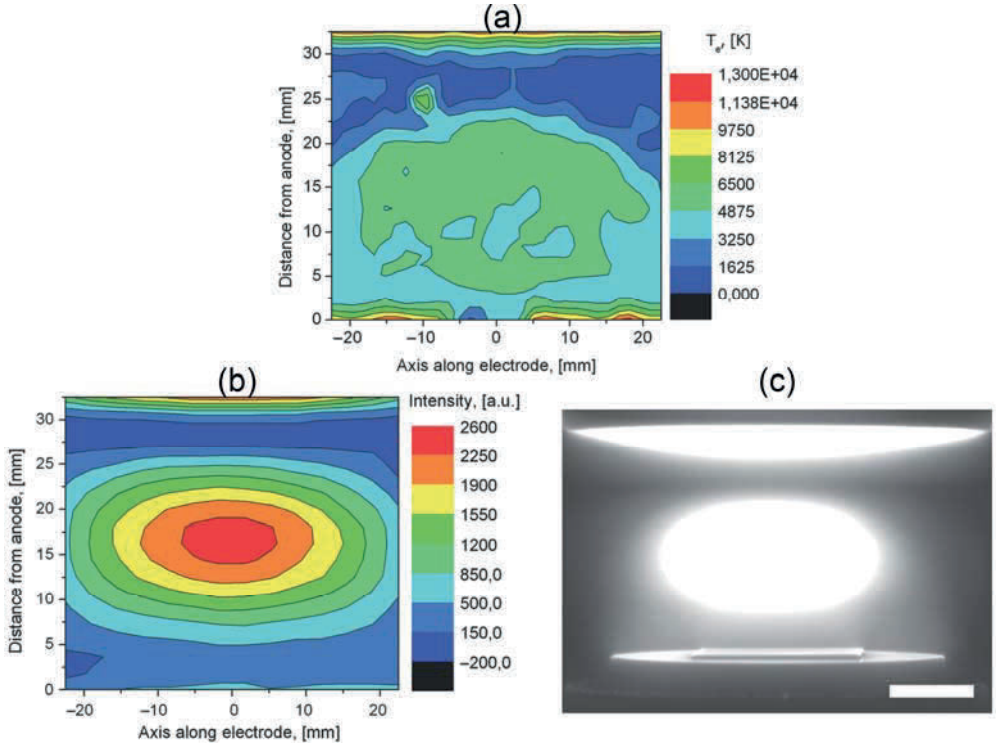

Fig. 9. *(a) - A spatial distribution of the electron temperature during the CVD; (b) - A spatial distribution of the emission intensity of the spectral line corresponding to C_2 species for typical deposition process; (c) - A CCD camera photograph of the substrate surrounded by DC discharge plasma captured at wavelength 514.5 nm with the optical interference filter (a scale bar is 10 mm).*

It was unexpectedly found that electron temperature distribution near the substrate is varied from the several to tens thousands of Kelvin in a very short distances. These temperature variations of plasma near the substrate surface may explain the formation of the rarely distributed well graphitized tubular structures incorporated into the nanodiamond films [125] and also could be connected with formation of the unusual chiral carbon nanoscrolls with a polygonal cross-section [126].

Conducted experimental plasma diagnostics allowed us to get general idea of what is happening in the certain activated CH_4/H_2 gas mixture, helped to optimize the equipment for reproducible deposition of different carbon nano- and microcrystalline materials and might be very useful for future studies (e.g., typical spatial distributions of C_2 emission line and electron temperature, leading to certain carbon material growth, might be used as an experimental results for verification of the theoretical models, that proposed to reveal main growth mechanisms and main growth species in plasma).

3.4 CONCLUSION OF CHAPTER 3

1. As a result of systematic inspection, the most appropriate CVD process parameters have been found for a reproducible deposition of different uniform carbon materials.

2. The activation of a methane-hydrogen gas mixture by the DC discharge leads to production C_2 dimers. The typical spatial distribution of the C_2 species in the plasma ball has been revealed. The appearance of this carbonaceous species in the gas mixture near a substrate surface correlates with the formation of graphite-like films. A condensation of carbon and a production of different types of carbon materials in gas phase are also possible.

3. The non-trivial variations of the electron temperature of the plasma were found near the substrate surface. This observation may help in understanding the formation of well graphitized needle-like structures in the nanodiamond and nanographite CVD films.

4 Graphitic nanomaterials

This chapter dedicated to the current research in the field of vapor deposition of few-layered graphene material. The structure of chapter is composed in such a way in order to show correlations between author's contribution (article **III**) and the main trends in this research area.

4.1 INTRODUCTION

Research on graphene has experienced explosive growth in the last few years. According to [127], several technical papers are published every day on the subject of graphene, making tracking all information related to graphene for researches extremely difficult or even impossible. Initial excitement for graphene came from its unusual linear dispersion of the π-band at the Fermi level, which gives rise to new physical properties. The isolation of single layer free-standing graphene from highly oriented pyrolytic graphite (HOPG) and the measurements of many exotic electronic properties of graphene have earned Konstantine (Kostya) S. Novoselov and Andre K. Geim the Physics Nobel Prize in 2010. The size of obtained graphene films was as small as ~ 10μm [5], but it was enough for revealing some fundamental properties. Obviously, the order of graphene size is not suitable for implementing unique material in industrial applications. For that reason many research groups over the globe (including our group) focus their efforts on invention the proper technique to manufacture large area graphene films, on discovering of new growth mechanisms. Having experience in deposition of different carbon materials, it was natural for our research group to evaluate the possibility of obtaining of this exciting material by a direct current CVD system and to reveal main growth features of their composition (see next paragraphs). Our research contribution to the graphene science goes back to the 2010, while now researchers continue solving other open questions. Among them one is related to the problems of obtaining large single-crystal graphene.

The initially reported micromechanical exfoliation of highly oriented pyrolytic graphite can only yield a small amount of tiny single-crystal graphene, limiting the applicability of this method. Recently developed CVD methods could produce large-size and uniform polycrystalline graphene [128], but the electronic properties of CVD graphene are degraded by domain boundaries [129]. Thus, the fabrication of large-size single-crystal graphene using CVD on transition metals, especially on Cu, Ni has attracted much interest among materials scientists [38,46,130]. In last year it was identified several advancements in the growth of Cu-based single-crystal graphene. For example, ~10μm sized self-arrayed single-crystal graphene

domains were fabricated by prepatterning graphite seeds on Cu [129]. The ~100-200μm sized hexagonal single-crystal graphene domains were made on melted Cu [131]. Submillimeter single-crystal graphene was successfully synthesized by preannealing Cu at atmospheric pressure or using a Cu enclosure for graphene growth. Finally, the growth of millimeter-sized single-crystal graphene was recently achieved on Pt [132] and Ni [133]. However, the facile synthesis of graphene with larger single-crystal domains on commercial Cu is desirable. Therefore, in spite of promising results, the study and development of high-quality CVD graphene is still on the way.

The discussed below experimental findings (partly presented in **III)** represent author contribution in 2010 to the "body of knowledge" of graphene deposition science.

4.2 EXPERIMENTAL

The single and few-layered graphene materials have been obtained by using the same low pressure direct current CVD equipment from activated hydrogen-methane gas mixture (see 3.2 paragraph). Standard Si (single crystalline; 500μm thick, 25×25mm^2 in sizes; (100) base plane) and Ni (polycrystalline; 500μm thick, 25×25mm^2 in sizes) have been used as substrates for investigation the graphite-like materials growth. A wide range of plasma parameters has been inspected in order to experimentally determine the possibilities for graphene growth. The best yield was obtained near the following specific conditions. The gas pressure *ca.* 10 *kPa*, total flow rate *ca.* 500 *SCCM* was maintained constant. The gas mixture contains about 5% of methane. This condition suits better, when the electrodes diameter is 50 mm and the inter-electrode distance is 50 mm. At the above mentioned conditions voltage between the electrodes is about 750 V and discharge current – about 7 A, while substrate temperature – about 1000°C. The deposition time was varied from 5 minutes to several hours providing the films with thicknesses in a wide range.

The obtained samples of CVD graphite films were characterized by Raman spectroscopy using U 1000 (Jobin Yvon) instrument with excitation by 514.5 nm Ar-ion laser. Scanning electron microscope (SEM) LEO 15500 (Zeiss) operated at 5 kV and Transmission electron microscope (TEM) TITAN 80-300 (FEI) with an imaging Cs corrector and operated at 80 kV were used for structural and surface topology investigations of the film samples.

The investigations were performed for as grown graphite-like films on Ni and Si substrates, for the films transferred from Ni onto polymer and glass (mica) substrates, and for the films freely suspended on the metal mesh (see **Fig.10**). For latter purpose Ni substrate has been etched in a mixture of sulfuric (H_2SO_4) and nitric (HNO_3) acids. Special attention has been paid to avoid formation of gas bubbles which are able to destroy thin film during the etching process.

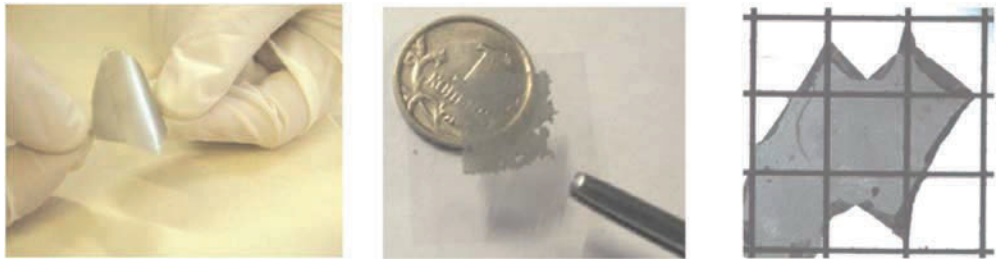

Fig. 10. *The photographs of the CVD graphite film of 20×20 mm² on polymer (**left**), of 10×10 mm² on glass (**center**), and on metallic mesh with 450×450 μm² cell size (**right**)*

4.3 RESULT AND DISCUSSION

Graphite-like material growth on Ni substrates. It was found, that deposition time extremely affects on morphology of graphite-like deposits. The plasma interaction with Ni substrate during less than one hour leads to graphite formation, which structural planes are primarily parallel to the substrate surface, while deposition during more than 1 hour leads to formation flakes-like structures with graphene plates, which are predominantly orthogonal to the substrate surface (as in **Fig.6a**). We limit our discussion by those which graphite-like material parallel to the substrate surface.

The surface of obtained films exhibits a wrinkled topology (see **Fig. 11**). We belief, that graphene forms flat at the surface during CVD and the wrinkles arise at the later cooling stage as a result of release of mechanical stress appeared due to difference in the thermal expansions of graphene film and Ni substrate.

Fig. 11. *SEM image showing wrinkled topology of few-layered graphene on a polycrystalline Ni substrate*

Our suggestions about structure and formation mechanism of the wrinkles well agree with the electron diffraction observations for free standing graphite films

allocated on a TEM mesh grid. While diffraction pattern detected for a flat film region corresponds to the well ordered graphite, additional reflections appeared in the pattern for a film area containing a wrinkle (see **Fig. 12**). This observation confirms that the wrinkles have the same atomic structure as the flat regions of the films but with direction of atomic layers nearly perpendicular to the film surface.

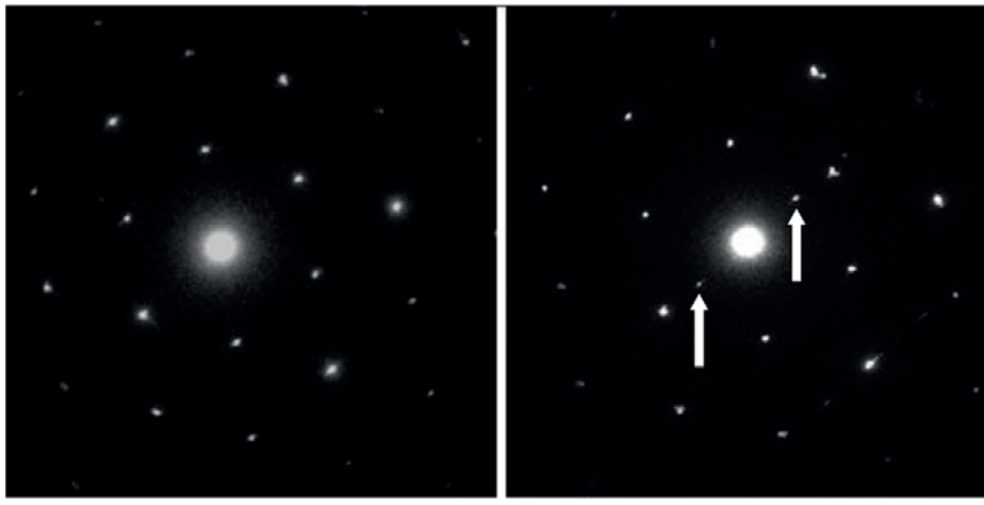

Fig. 12. *The electron micro-diffraction patterns obtained for a flat region on few-layered graphene surface (**left**) and for a region, containing a single wrinkle (**right**). Two additional reflections are indicated by the arrows*

It was found that graphene formation and appearance of the wrinkles does not correlate with crystallography orientation of Ni substrate. It was especially evident from the SEM image (see **Fig.13**). A micron-sized Ni single crystal shown in this image was produced at initial stage of the deposition process as a result of crystallization of substrate material melted due to occasional discharge arcing. SEM observation shows that all facets of the Ni crystal are covered by graphene film independently on their crystallography orientation. The wrinkles formation also looks independent on crystallography orientation of surfaces of the Ni single crystal.

One might suppose that the wrinkles can be stem from the interval between adjacent grains (grain "connection") of polycrystalline Ni substrate. However, in **Fig.13** can be seen clearly that wrinkles appear on the flat surface of the Ni single crystal, on the place were no any grain connections. This observation additionally confirms the proposed genesis of the wrinkles.

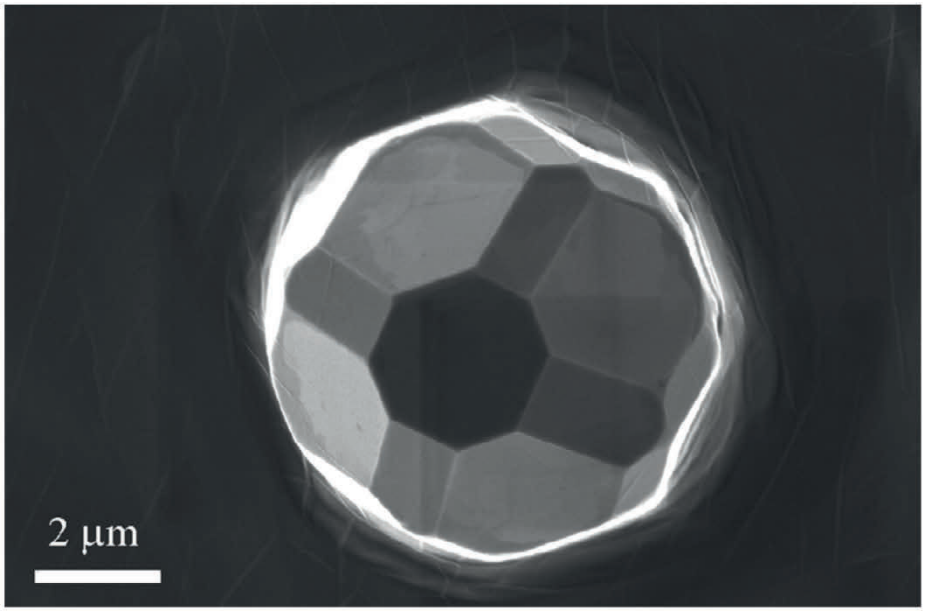

Fig. 13. *SEM image showing a Ni single crystal and adjacent polycrystalline substrate covered by graphite film*

Additionally to the wrinkles a formation of blisters on the surface of the CVD graphite films was observed. These blisters appear to be growing in size after unloading of samples from the reactor chamber to air. The blisters with the size in the range of a few to hundreds micrometers are typically formed during few hours exposure in air at room temperature. The examples of the blisters are shown in **Fig.14.**

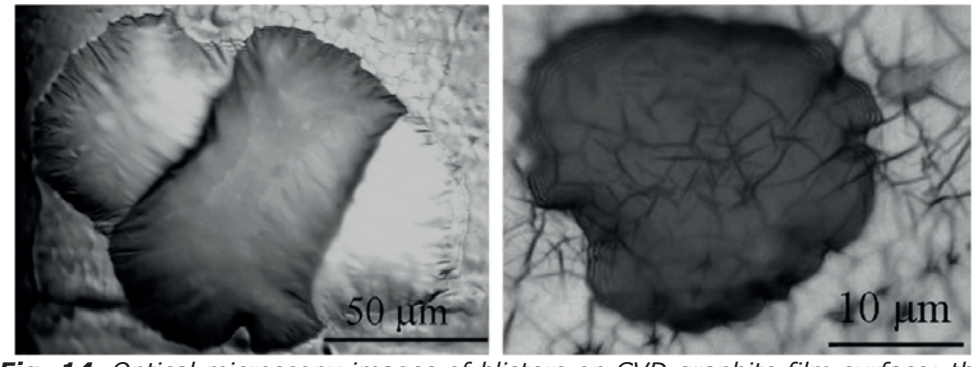

Fig. 14. *Optical microscopy images of blisters on CVD graphite film surface: the three joined blisters (**left**) and a blister with transparent wall (**right**)*

The shapes and genesis of the blisters unambiguously show a presence of a gaseous phase inside at a pressure exceeding external atmosphere. It seems impossible to assume that the blisters are filled by any liquid. The light interference fringes are clearly seen for blisters with the thinnest walls transparent for light.

Formation of the blisters is an evidence for graphite layers exfoliation. Such kind of phenomena was observed also by TEM. **Fig.15** shows an example of a high resolution TEM (HRTEM) image with a single graphene layer detached from the multilayer graphite film material. Number of graphene layers in different blisters was evaluated by Raman spectroscopy. The spectra in **Fig.16** demonstrate shape difference for 2D second order Raman band for the blisters shown in microphotographs of **Fig.14.**

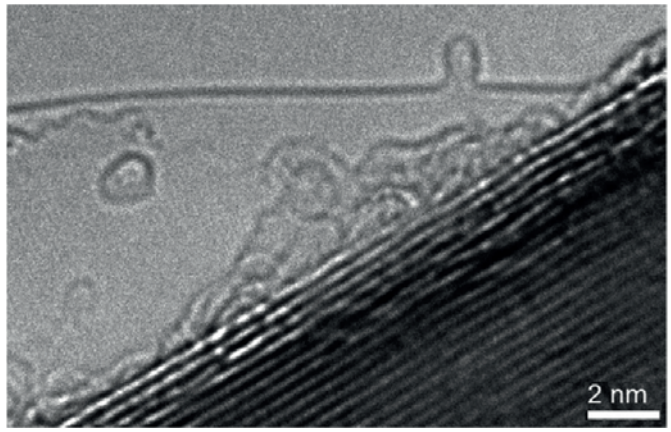

Fig. 15. *HRTEM image with a single graphene layer detached from the CVD graphite film*

According to [134,135], Raman spectra for transparent blister shown in right panel of **Fig.14** corresponds to 1 or 2 graphene layer (spectrum 3) while adjacent area of the CVD film contains more than 10 layers (spectrum 1); the spectrum 2 corresponds to 3 atomic layers, but spectrum 4 may be assigned to rather thick turbostratic graphite.

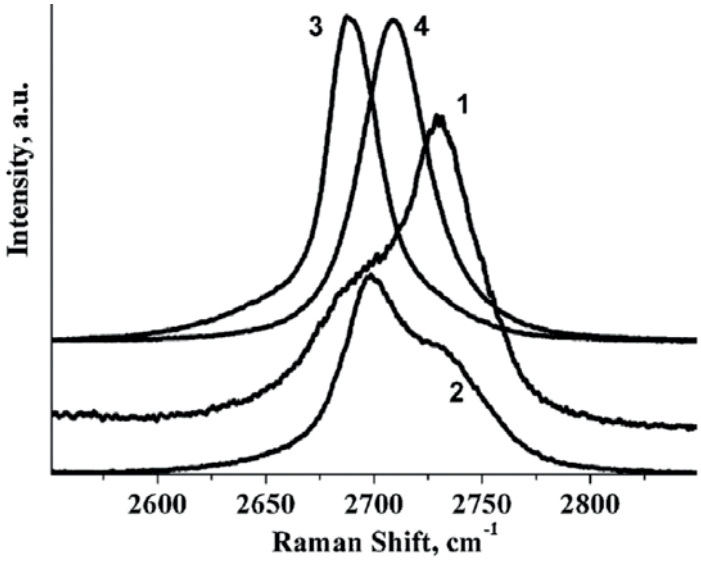

Fig. 16. *The second order 2D bands in the Raman spectra measured for different areas in the films shown in Fig.13:* ***1*** *– outside the transparent blister in the right panel;* ***2****–on top of the left blister in the left panel;* ***3*** *– on top of the blister in right panel;* ***4*** *– on top of right blister in the left panel*

Origin of the gas filled blisters may be explained by a presence of hydrogen in-between the atomic layers composing the CVD graphite films. The hydrogen atoms are trapped between the graphene layers, probably during film formation by carbon atoms condensation from hydrogen-methane plasma. Van der Walls attraction between the layers impress the trapped hydrogen atoms enforcing formation of the blisters with time at ambient conditions (room temperature and normal atmosphere pressure). This process is stimulated by high mobility of hydrogen and low gas permeability of graphene atomic layers [136]. The resultant blisters are very stable and preserve high inner pressure for more than a few months. However, depressurization of the blisters was observed in a course of scanning probe microscopy studies due to mechanical damages of the blister walls and high pressure differences.

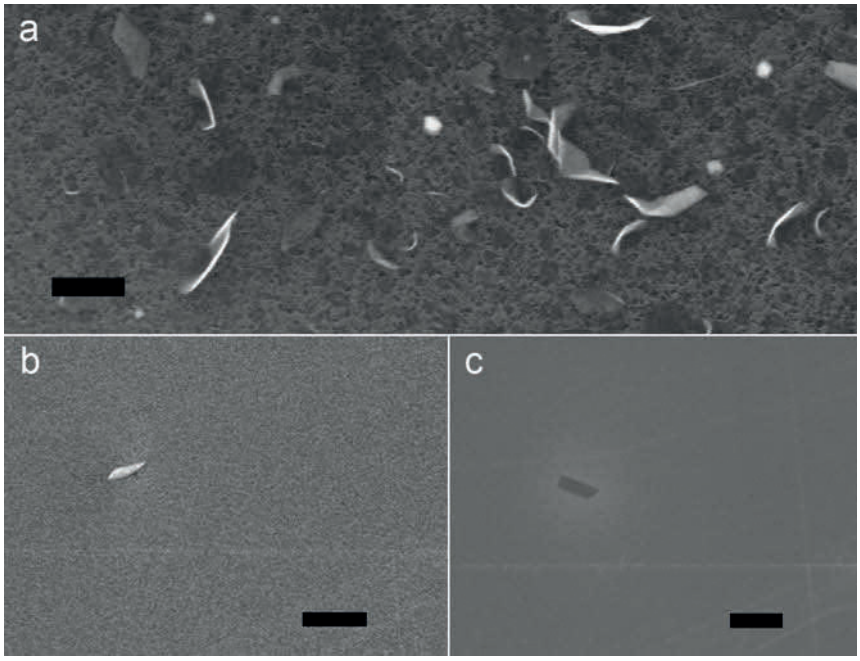

Fig.17. *SEM images showing perpendicular orientation of as grown few-layered graphene on Si substrate: (a) – shows their random appearance (scale bar is 200nm); (b) and (c) – show their poor fixation on the substrate (scale bars are 2 μm)*

Graphite-like material growth on Si substrates. In most cases graphite-like materials appear to have graphene base plane's orientation perpendicular to the Si substrate surface (see **Fig.17**). Such perpendicular orientation makes them unsteady on the substrate. For example, particular few-layered graphene sheets may easily fall down during electron scanning (compare **Fig.17b** and **Fig.17c**). It should be noted, that several experiments revealed some traces of possible graphene appearance on Si substrates (see wrinkles appearance in **Fig.18**). These observations indicate graphene growth mechanisms different from commonly accepted model. Latter model implies, that, at the first stage, carbon dissolves into the metal substrate; at the second stage, carbon is forced to precipitate out of the substrate caused by cooling procedure; and at the final stage, the precipitated carbon atoms merge and compose graphene layers [46]. Our experimental observations witness ability of graphene formation by direct condensation of carbon from the gaseous environment. In this case graphene formation is possible on different substrates except commonly used metals (Ni, Cu, etc.). However obtaining of reproducible results on graphene formation via carbon condensation requires appropriate CVD process optimization which was not achieved in frame of this work. Only limited results were obtained indicating principal ability formation of large scale graphene on non-metallic substrates.

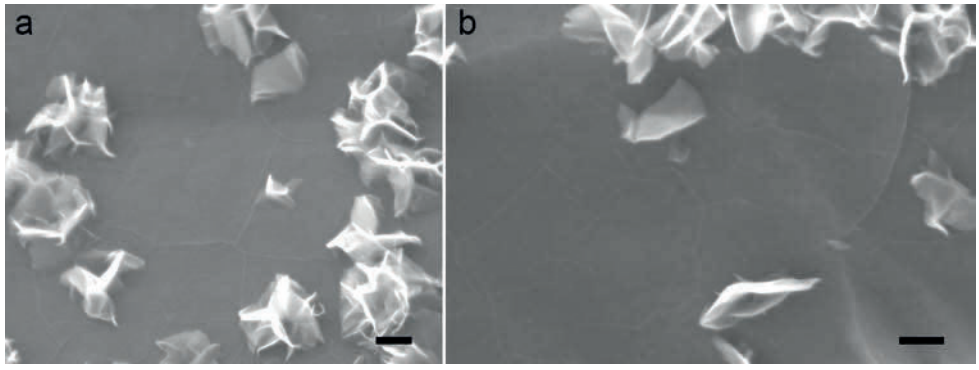

Fig.18. *SEM images showing typical graphene traces on Si substrates. Scale bars are 200nm*

4.4 CONCLUSION OF CHAPTER 4

1. Appropriate CVD process parameters have been found for a reproducible deposition of few-layered graphene on Ni substrates.

2. The surface of few-layered graphene films obtained by plasma-enhanced CVD possesses a wrinkled topology. It has been proposed that graphene films are originally flat and surface wrinkles are the result of mechanical stress appeared at interface between film and substrate during subsequent cooling.

3. The gaseous blisters were found on the graphite film after their exposure in air at room temperature. Genesis of the gaseous blisters formed in CVD grown films is assigned to hydrogen trapped in between graphene layers during film formation.

5 Nano- and microdiamonds

This chapter dedicated to the current research in the field of vapor deposition of single-crystal diamond materials. The structure of chapter is composed in such a way in order to show correlations between author's contributions (articles **II, IV, V**) and main trends in this research area.

5.1 INTRODUCTION

Exceptional mechanical, thermal, optical, and electronic properties make diamond very attractive for numerous applications. However, in some cases the exploitation of these advantages is hampered by difficulties in obtaining the desired geometry of diamonds in nano- and micro- scales. In particular, tip-shaped diamonds are desired for different types of scanning probe microscopes [137,138], indenters [139], nanolithography [140,141], magnetic diamond sensors [142]. To obtain diamond tips, it has been proposed to use micromachining of single crystals [143], plasma etching of polycrystalline diamond films [144–146], and chemical vapor deposition (CVD) growth on tip-shaped [147,148] or pyramidal pit etched substrates [149,141]. These technologies are able to provide advantageous results. However, most of these methods provide tips with polycrystalline or highly defective apexes having rather large radii of curvature. The micromachined single crystal diamond tips are very difficult and expensive to fabricate with reproducible geometry. Therefore, in spite of promising results, the study and development of diamonds with specified form, particularly, tip-shaped is still on the way.

It is well known, that the diamond-like CVD films usually possess a columnar growth structure, which is typical of the growth morphology from H_2/CH_4 plasmas and reflects the van der Drift growth mechanism [15]. Briefly this growth van der Drift principle ("evolutionary selection") [150] can be explained as follows. A great number of the crystals with random orientations are first formed on the seeded support in the very early stage. These crystals can grow in all possible directions. Upon growth, the crystals touch each other. When two crystals meet, the growth front of a less steep crystal touches the flank of a steeper one and thereafter stops growing, whereas the steeper one continues to grow. Similarly, when this steeper crystal meets a much steeper crystal, it ends in the flank of the much steeper one and the latter can grow further. As a consequence of such "evolutionary selection" processes, many crystals are embedded under the growing layer, while only those crystals with their fastest growth direction vertical to the support surface survive.

For the best of our knowledge, there are only few research groups, including ours, which focus their attention on detailed investigation of growth mechanisms of the columnar diamonds, at least, with a view to control diamond column morphology. In this study some interesting mechanisms of CVD columnar diamond growth has been revealed, which open the easiest way for mass production of diamond needles with arbitrarily shape. Some of obtained results are presented below.

5.2 EXPERIMENTAL

The experiments were carried out using the same CVD equipments described above (see paragraph 3.2). The textured polycrystalline diamond films were grown from a hydrogen-methane gas mixture activated by a DC discharge. The single-crystal 500 μm thick Si(100) 25×25 mm^2 wafers were used as substrates. The deposition temperature of substrate surface was kept near 900°C (monitored by an optical pyrometer). The total gas flow rate 250 sccm and the total pressure 100 mbar were kept constant during deposition. The methane concentration in the gas mixture was 3% to achieve a film with different structural composition - the mixture of nano- and micro- sized diamonds (in the same film).

A thermal oxidation of the diamond films was performed in an oven with the adjustable temperature in an air under a normal pressure. The as-deposed and oxidized samples were studied by the Raman spectroscopy using the Renishaw inVia Raman Microscope with the excitation at 514,5 nm and a 50 × optical magnification. The surface morphology of the CVD films was monitored by SEM using a LEO 1550 (Zeiss) microscope operated at 5 kV of an accelerating voltage in a backscattering geometry.

5.3 RESULT AND DISCUSSION

Fig.19 shows typical SEM images of the CVD films obtained at the above mentioned conditions. The films consist of a mixture of micrometer sized crystallites, having well developed rectangular (100) facets on the film surface, and submicrometer and nanometer sized species with shapes which cannot be resolved by the SEM (**Fig.19a**). Raman spectroscopy analysis reveals that the films consist of diamond crystallites of different sizes, graphitic inclusions, and amorphous carbon.

The CVD films of this type were oxidized by exposure in normal air atmosphere at a temperature of 680 °C for 5 h. The oxidized CVD film consists of the pyramid shaped diamond crystallites oriented by their apexes toward the substrate surface. In this orientation the crystallites are weakly connected to the substrate and some of

them are fallen down on their sides (see **Fig.19c**). The pyramid shaped crystallites can be detached easily either by a gentle pressing or by a scratching with tweezers.

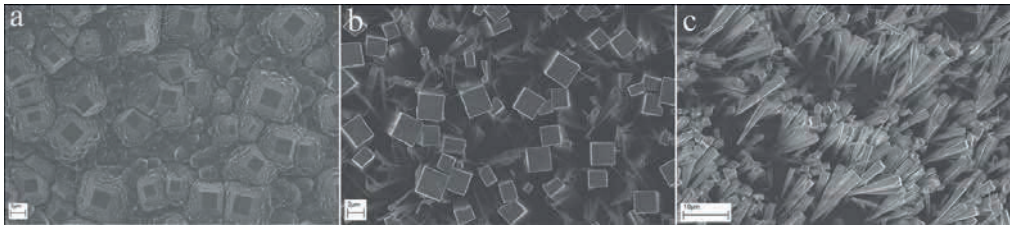

Fig.19. *(**a–c**) The SEM images of CVD diamond film obtained with CH4 concentration of 3% for 5 hours growth: (**a**) - as-grown; (**b**) - oxidized during 2 hours at 680°C in air; (**c**) - the diamond crystallites detached from the substrate*

Curve 1 in **Fig.20** shows the Raman spectrum of the pristine CVD diamond film. This spectrum demonstrates a strong 1330 cm^{-1} band corresponding to the micro-sized diamond crystallites and the Raman lines related to the nanodiamond and graphitic phases presented in the film in significant amount. The spectrum of the same film after an exposure in the air atmosphere at 680°C during 2 hours (curve 2 in **Fig.20**) demonstrates an intense narrow line at 1330 cm^{-1}, and only a weak wide band at 1580 cm^{-1} representing a remaining amorphous carbon in a little amount. It is evident also from a comparison of the spectra presented in **Fig.20** that the thermal oxidation reduces the width of the "diamond" Raman band at 1330 cm^{-1} from 18 cm^{-1} down to 5 cm^{-1}. Such a narrowing might be explained by two reasons: (i) an etching of the most defective diamond micro-crystallites, and (ii) a reduction of the mechanical stress induced by the nano-diamond phase presence. The removal of a substantial part of graphitic and nanodiamond species during the oxidation is in good agreement with the published data [151].

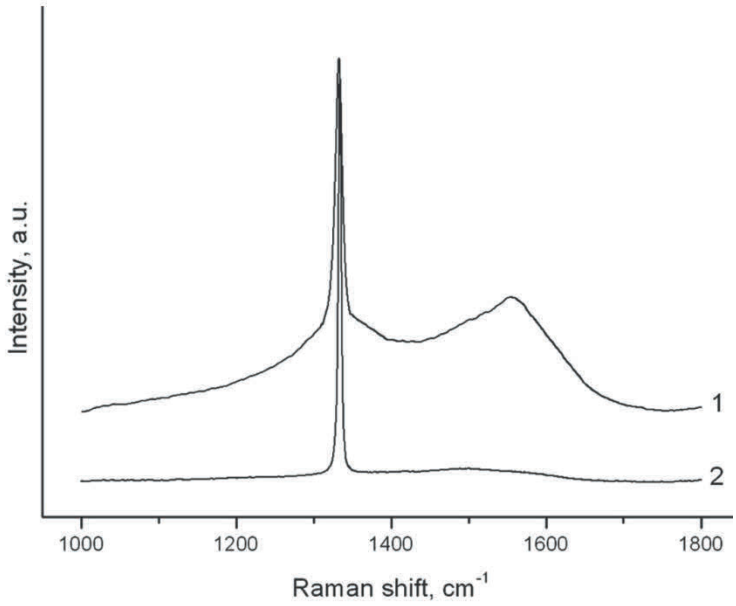

Fig.20. *The Raman spectra of the same film: as-grown –* ***curve 1****; after oxidation during 2 hours at 680°C in air –* ***curve 2***

The sizes of the diamond single crystal pyramids obtained at the described condition are about 10–15μm in length and have about 4–5 μm edges of the rectangular base plane. These planes are practically squares that correspond to the (100) diamond facet. Oxidation does not produce any significant changes in the shape and flatness of these base planes. The apexes of the pyramids have a typical radius of curvature in the range of 20–2 nm. The last number corresponds to the smallest size of thermodynamically stable diamond [152,153].

Use of the CVD technology allows very easy and inexpensive mass production of this type of diamond tips which may be attractive for different applications. In paper **IV** we demonstrated the possibility for efficient application of the diamond needles as atomic force microscopy (AFM) probes. The AFM probes were manufactured by attaching the diamond tips to standard silicon and silicon-nitride cantilevers. **Fig.21a** shows a SEM image of the AFM probe with a diamond tip glued to a silicon cantilever by an epoxy. Similar diamond AFM probes were tested with different samples. **Fig.21b** and **c** show the comparative test made using a sample of a TiN film deposited onto polished (Ra<10 nm) glass by magnetron sputtering. The TiN film thickness was about 200 nm.

In the test measurements, scanning of the TiN sample surface was performed by gradually increasing the lateral resolution up to the moment when the resulting AFM images became blurred. The resolution increase was obtained by reducing size of the scanned area with the same number 500×500 points in the scans, and the image blurring corresponds to the situation when the neighboring points in the scan have identical parameters. An example of such a blurred image obtained using a standard Si probe is shown in **Fig.21c. Fig.21b** shows the AFM image obtained

under the same conditions, but using the diamond tip probe. The improvement of AFM imaging with the use the diamond probe is evident.

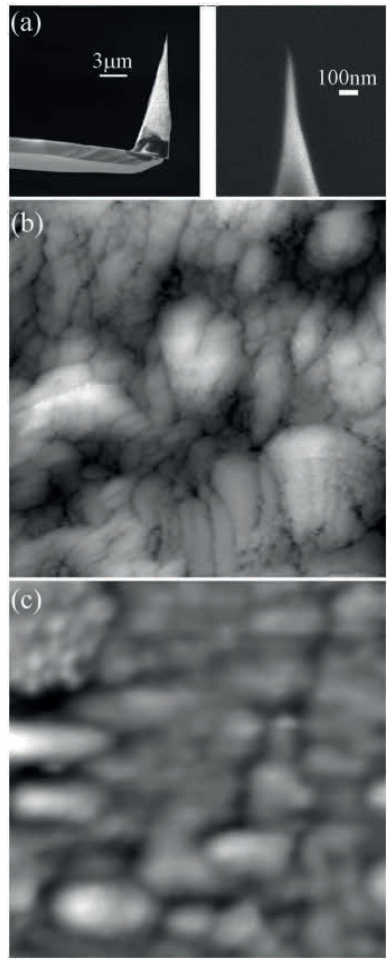

Fig.21. *SEM image of an AFM probe made by gluing a single crystal diamond tip to a silicon cantilever (**a**). AFM images obtained for the TiN film sample using the diamond probe (**b**) and the common silicon probe (**c**). The size of the AFM scans is 300×300 nm²*

Other advantages of the diamond probes were found in the test measurements made for the biological objects. Due to the hydrophobicity of the surface, the diamond probes show a much better efficiency (higher resolution combined with much longer life time) in comparison with typical silicon probes. The chemical inertness of diamond is an important factor providing better imaging performance of the diamond AFM probes. The excellent wear resistance of diamond can play a significant role in other applications.

It should be noted, that small changes of plasma growth parameters significantly affect on the diamond needle morphology. In particularly, tiny

deviation from mentioned plasma parameters leads to noticeable changing of the convergence angle (see **Fig.22**). Such control might be very useful for deposition extraordinarily shaped diamond structures. The crystallites shown in **Fig. 22**, for example, were obtained in a CVD process with a sequence of variations of substrate temperature. This leads to variation of angle of the pyramidal crystallite shape.

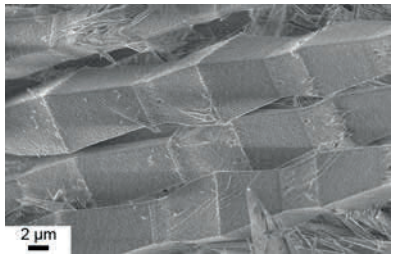

Fig.22. *SEM image of needle-like diamonds obtained in case of tiny periodic changes of deposition parameters*

5.4 CONCLUSION OF CHAPTER 5

1. Appropriate CVD process parameters have been found for a reproducible deposition of nanodiamond films with embedded single crystal diamonds of micrometer size with regular pyramidal shape having a square base plane and a tiny pointed apex.

2. The methods, based on CVD film growth and selective oxidation, which provide inexpensive mass production of the diamond pyramidal tips suitable for different applications have been developed.

3. As an example, the possibility for efficient application of the diamond tips as AFM probes has been demonstrated.

6 Conclusion and outlook

This thesis provides demonstrations of different carbon structures together with the impact of chemical vapor deposition of these materials. We have studied the chemical vapor deposition in wide range of process parameters and reveal some peculiarities in formation of carbon solids from methane-hydrogen gas mixture activated by DC discharge. Particularly, the chemical deposition of few-layered graphene, pure nanodiamond, microdiamond films, and diamond films, containing the pyramidal diamond crystallites from hydrogen/methane gas mixture were experimentally investigated.

CVD provides several advantages in material science as a unique deposition method for obtaining different kinds of carbon structures. I believe in near future the research on CVD could allow controlled production of large-size single-crystal graphene, bi- and few-layered graphene with different stacking order, diamond deposition at low temperature and ambient pressure, and other challenging carbon-related composite materials. With the current rapid rate of progress, it should not be too long before carbon related CVD technology begins to make a significant impact in many areas of modern science and technology.

References

1. J. Wright, S. Guceri, Y. G. Gogotsi, and V. Kuznetsov, *Nanoengineered Nanofibrous Materials*, NATO Science Series II: Mathematics, Physics and Chemistry (Springer, 2004).
2. M. He, S. Vasala, H. Jiang, M. Karppinen, E. I. Kauppinen, M. Niemela, and J. Lehtonen, "Growth and surface engineering of vertically-aligned low-wall-number carbon nanotubes," CARBON **50**, 4750–4754 (2012).
3. H. Kroto, J.Heath, S. Orbien, R. Curl, and R. Smalley, "C-60 - Buckminsterfullerene," NATURE **318**, 162–163 (1985).
4. A. Moisala, A. Nasibulin, and E. Kauppinen, "The role of metal nanoparticles in the catalytic production of single-walled carbon nanotubes - a review," JOURNAL OF PHYSICS-CONDENSED MATTER **15**, S3011–S3035 (2003).
5. K. Novoselov, A. Geim, S. Morozov, D. Jiang, Y. Zhang, S. Dubonos, I. Grigorieva, and A. Firsov, "Electric field effect in atomically thin carbon films," SCIENCE **306**, 666–669 (2004).
6. K. Okada, "Plasma-enhanced chemical vapor deposition of nanocrystalline diamond," SCIENCE AND TECHNOLOGY OF ADVANCED MATERIALS **8**, 624 (2007).
7. H. O. Pierson, *Handbook of Carbon, Graphite, Diamond, and Fullerenes: Properties, Processing, and Applications*, Materials Science and Process Technology Series (Noyes Publications, 1993).
8. R. J. Kee, G. H. Evans, and M. E. Coltrin, "Application of Supercomputers To Model Fluid Transport and Chemical Kinetics in Chemical Vapor Deposition Reactors," in *Supercomputer Research in Chemistry and Chemical Engineering*, pp. 334–352.
9. J. Schrier, "Carbon Dioxide Separation with a Two-Dimensional Polymer Membrane," ACS APPLIED MATERIALS & INTERFACES **4**, 3745–3752 (2012).
10. D. Tomanek, "Carbon-based nanotechnology on a supercomputer," JOURNAL OF PHYSICS-CONDENSED MATTER **17**, R413–R459 (2005).
11. K. E. Spear and J. P. Dismukes, *Synthetic Diamond: Emerging CVD Science and Technology*, Electrochemical Society Series (Wiley, 1994).
12. T. D. Burchell, *Carbon Materials for Advanced Technologies*, Referex Engineering (Pergamon, 1999).
13. R. Baughman, A. Zakhidov, and W. de Heer, "Carbon nanotubes - the route toward applications," SCIENCE **297**, 787–792 (2002).

14. K. De Jong and J. Geus, "Carbon nanofibers: Catalytic synthesis and applications," CATALYSIS REVIEWS-SCIENCE AND ENGINEERING **42**, 481–510 (2000).
15. D. Gruen, "Nanocrystalline diamond films," ANNUAL REVIEW OF MATERIALS SCIENCE **29**, 211–259 (1999).
16. M. Hiramatsu and M. Hori, *Carbon Nanowalls* (Springer Vienna, 2009).
17. A. Jorio, M. S. Dresselhaus, R. Saito, and G. Dresselhaus, *Raman Spectroscopy in Graphene Related Systems* (Wiley, 2011).
18. J. Robertson, "Diamond-like amorphous carbon," MATERIALS SCIENCE & ENGINEERING R-REPORTS **37**, 129–281 (2002).
19. V. Singh, D. Joung, L. Zhai, S. Das, S. I. Khondaker, and S. Seal, "Graphene based materials: Past, present and future," PROGRESS IN MATERIALS SCIENCE **56**, 1178–1271 (2011).
20. S. Stankovich, D. A. Dikin, G. H. B. Dommett, K. M. Kohlhaas, E. J. Zimney, E. A. Stach, R. D. Piner, S. T. Nguyen, and R. S. Ruoff, "Graphene-based composite materials," NATURE **442**, 282–286 (2006).
21. P. W. Atkins and J. De Paula, *Atkins' Physical Chemistry* (Oxford University Press, 2006).
22. A. W. Hull., "A New Method of X-Ray Crystal Analysis," PHYSICAL REVIEW **10**, 661–696 (1917).
23. D. S. Knight and W. B. White, "Characterization of diamond films by Raman spectroscopy," JOURNAL OF MATERIALS RESEARCH **4**, 385–393 (1989).
24. M. Dresselhaus, G. Dresselhaus, and A. Jorio, "Unusual properties and structure of carbonnanotubes," ANNUAL REVIEW OF MATERIALS RESEARCH **34**, 247–278 (2004).
25. H. Kroto, A. Allaf, and S. Balm, "C60 - Buckmisterfullerene," CHEMICAL REVIEWS **91**, 1213–1235 (1991).
26. R. Taylor and D. Walton, "The chemistry of fullerences," NATURE **363**, 685–693 (1993).
27. E. Thostenson, Z. Ren, and T. Chou, "Advances in the science and technology of carbon nanotubes and their composites: a review," COMPOSITES SCIENCE AND TECHNOLOGY **61**, 1899–1912 (2001).
28. O. V. Kharissova and B. I. Kharisov, "Less-Common Nanostructures in the Forms of Vegetation," INDUSTRIAL & ENGINEERING CHEMISTRY RESEARCH **49**, 11142–11169 (2010).
29. M. U. Niemann, S. S. Srinivasan, A. R. Phani, A. Kumar, D. Y. Goswami, and E. K. Stefanakos, "Nanomaterials for Hydrogen Storage Applications: A Review," JOURNAL OF NANOMATERIALS **2008**, 950967 (2008).
30. M. S. Dresselhaus, *Graphite Fibers and Filaments*, Springer Series in Materials Science (Springer-Verlag, 1988).
31. S. Dresselhaus, G. Dresselhaus, and P. C. Eklund, *Science of Fullerenes and Carbon Nanotubes: Their Properties and Applications* (Elsevier Science, 1996).

32. P. W. Stephens, *Physics & Chemistry of Fullerenes: A Reprint Collection*, Advanced Series in Fullerenes (World Scientific, 1993).
33. A. Oberlin, "Carbonization and graphitization," CARBON **22**, 521–541 (1984).
34. M. Inagaki, S. Harada, T. Sato, T. Nakajima, Y. Horino, and K. Morita, "Carbonization of polyimide film kapton," CARBON **27**, 253–257 (1989).
35. S. Zhao, Z.-Q. Shi, C.-Y. Wang, and M.-M. Chen, "Structure and surface elemental state analysis of polyimide resin film after carbonization and graphitization," JOURNAL OF APPLIED POLYMER SCIENCE **108**, 1852–1856 (2008).
36. O. A. Shenderova and D. M. Gruen, *Ultrananocrystalline Diamond: Synthesis, Properties and Applications*, Micro and Nano Technologies (Elsevier Science, 2012).
37. J. E. Butler and A. V. Sumant, "The CVD of nanodiamond materials," CHEMICAL VAPOR DEPOSITION **14**, 145–160 (2008).
38. A. Cassell, J. Raymakers, J. Kong, and H. Dai, "Large scale CVD synthesis of single-walled carbon nanotubes," JOURNAL OF PHYSICAL CHEMISTRY B **103**, 6484–6492 (1999).
39. G. Che, B. Lakshmi, C. Martin, E. Fisher, and R. Ruoff, "Chemical vapor deposition based synthesis of carbon nanotubes and nanofibers using a template method," CHEMISTRY OF MATERIALS **10**, 260–267 (1998).
40. C. Cheung, A. Kurtz, H. Park, and C. Lieber, "Diameter-controlled synthesis of carbon nanotubes," JOURNAL OF PHYSICAL CHEMISTRY B **106**, 2429–2433 (2002).
41. J. Kong, A. Cassell, and H. Dai, "Chemical vapor deposition of methane for single-walled carbon nanotubes," CHEMICAL PHYSICS LETTERS **292**, 567–574 (1998).
42. Y. Li, W. Kim, Y. Zhang, M. Rolandi, D. Wang, and H. Dai, "Growth of single-walled carbon nanotubes from discrete catalytic nanoparticles of various sizes," JOURNAL OF PHYSICAL CHEMISTRY B **105**, 11424–11431 (2001).
43. Z. L. Tsakadze, I. Levchenko, K. Ostrikov, and S. Xu, "Plasma-assisted self-organized growth of uniform carbon nanocone arrays," CARBON **45**, 2022–2030 (2007).
44. Q. Yang, C. Xiao, W. Chen, and A. Hirose, "Selective growth of diamond and carbon nanostructures by hot filament chemical vapor deposition," DIAMOND AND RELATED MATERIALS **13**, 433–437 (2004).
45. X. Li, W. Cai, L. Colombo, and R. S. Ruoff, "Evolution of Graphene Growth on Ni and Cu by Carbon Isotope Labeling," NANO LETTERS **9**, 4268–4272 (2009).
46. A. N. Obraztsov, "Chemical vapour deposition Making graphene on a large scale," NATURE NANOTECHNOLOGY **4**, 212–213 (2009).

47. A. Reina, X. Jia, J. Ho, D. Nezich, H. Son, V. Bulovic, M. S. Dresselhaus, and J. Kong, "Large Area, Few-Layer Graphene Films on Arbitrary Substrates by Chemical Vapor Deposition," NANO LETTERS **9**, 30–35 (2009).
48. D. Wei, Y. Liu, Y. Wang, H. Zhang, L. Huang, and G. Yu, "Synthesis of N-Doped Graphene by Chemical Vapor Deposition and Its Electrical Properties," NANO LETTERS **9**, 1752–1758 (2009).
49. J. R. Rabeau, A. Stacey, A. Rabeau, S. Prawer, F. Jelezko, I. Mirza, and J. Wrachtrup, "Single nitrogen vacancy centers in chemical vapor deposited diamond nanocrystals," NANO LETTERS **7**, 3433–3437 (2007).
50. A. M. Schrand, S. A. C. Hens, and O. A. Shenderova, "Nanodiamond Particles: Properties and Perspectives for Bioapplications," CRITICAL REVIEWS IN SOLID STATE AND MATERIALS SCIENCES **34**, 18–74 (2009).
51. J. E. Butler, Y. A. Mankelevich, A. Cheesman, J. Ma, and M. N. R. Ashfold, "Understanding the chemical vapor deposition of diamond: recent progress," JOURNAL OF PHYSICS-CONDENSED MATTER **21**, 364201 (2009).
52. T. Farouk, B. Farouk, and A. Fridman, "Computational Studies of Atmospheric-Pressure Methane-Hydrogen DC Micro Glow Discharges," IEEE TRANSACTIONS ON PLASMA SCIENCE **38**, 73–85 (2010).
53. F. J. Gordillo-Vazquez and J. M. Albella, "Distinct nonequilibrium plasma chemistry of C_2 affecting the synthesis of nanodiamond thin films from C_2H_2 (1%)/H_2/Ar-rich plasmas," Journal of Applied Physics **94**, 6085–6090 (2003).
54. P. May, J. Harvey, J. Smith, and Y. Mankelevich, "Reevaluation of the mechanism for ultrananocrystalline diamond deposition from Ar/CH_4/H_2 gas mixtures," JOURNAL OF APPLIED PHYSICS **99**, 104907 (2006).
55. M. J. Allen, V. C. Tung, and R. B. Kaner, "Honeycomb Carbon: A Review of Graphene," CHEMICAL REVIEWS **110**, 132–145 (2010).
56. M. Dresselhaus, G. Dresselhaus, R. Saito, and A. Jorio, "Raman spectroscopy of carbon nanotubes," PHYSICS REPORTS-REVIEW SECTION OF PHYSICS LETTERS **409**, 47–99 (2005).
57. A. Ferrari and J. Robertson, "Interpretation of Raman spectra of disordered and amorphous carbon," PHYSICAL REVIEW B **61**, 14095–14107 (2000).
58. F. Tuinstra and J. L. Koenig, "Raman Spectrum of Graphite," The Journal of Chemical Physics **53**, 1126–1130 (1970).
59. D. Beeman, J. Silverman, R. Lynds, and M. R. Anderson, "Modeling studies of amorphous carbon," PHYSICAL REVIEW B **30**, 870–875 (1984).
60. R. Nemanich and S. Solin, "1st-order and 2nd-order Raman-scattering from finite-size crystals of graphite," PHYSICAL REVIEW B **20**, 392–401 (1979).
61. A. C. Ferrari, J. C. Meyer, V. Scardaci, C. Casiraghi, M. Lazzeri, F. Mauri, S. Piscanec, D. Jiang, K. S. Novoselov, S. Roth, and A. K. Geim, "Raman spectrum of graphene and graphene layers," PHYSICAL REVIEW LETTERS **97**, 187401 (2006).

62. M. S. Dresselhaus, A. Jorio, and R. Saito, "Characterizing Graphene, Graphite, and Carbon Nanotubes by Raman Spectroscopy," ANNUAL REVIEW OF CONDENSED MATTER PHYSICS **1**, 89–108 (2010).
63. A. Ferrari and J. Robertson, "Origin of the 1150-cm^{-1} Raman mode in nanocrystalline diamond," PHYSICAL REVIEW B **63**, 121405(R) (2001).
64. S. Sharma, H. Mao, P. Bell, and J. Xu, "Measurement of stress in diamond anvils with micro-Raman spectroscopy," JOURNAL OF RAMAN SPECTROSCOPY **16**, 350–352 (1985).
65. A. A. Balandin, S. Ghosh, W. Bao, I. Calizo, D. Teweldebrhan, F. Miao, and C. N. Lau, "Superior thermal conductivity of single-layer graphene," NANO LETTERS **8**, 902–907 (2008).
66. A. N. Obraztsov, A. V. Tyurnina, E. A. Obraztsova, A. A. Zolotukhin, B. Liu, K.-C. Chin, and A. T. S. Wee, "Raman scattering characterization of CVD graphite films," CARBON **46**, 963–968 (2008).
67. A. Ferrari, "Determination of bonding in diamond-like carbon by Raman spectroscopy," DIAMOND AND RELATED MATERIALS **11**, 1053–1061 (2002).
68. P. E. Champness, *Electron Diffraction in the Transmission Electron Microscope*, Microscopy Handbooks (Bios Scientific, 2001).
69. X. Zou, S. Hovmöller, and P. Oleynikov, *Electron Crystallography: Electron Microscopy and Electron Diffraction*, International Union of Crystallography Texts on Crystallography (OUP Oxford, 2011).
70. D. B. Williams and C. B. Carter, *Transmission Electron Microscopy: A Textbook for Materials Science*, (Plenum Press, 1996).
71. N. Xu, J. Chen, and S. Deng, "Effect of heat treatment on the properties of nano-diamond under oxygen and argon ambient," DIAMOND AND RELATED MATERIALS **11**, 249–256 (2002).
72. M. Monthioux, B. Smith, B. Burteaux, A. Claye, J. Fischer, and D. Luzzi, "Sensitivity of single-wall carbon nanotubes to chemical processing: an electron microscopy investigation," CARBON **39**, 1251–1272 (2001).
73. J. C. Meyer, A. K. Geim, M. I. Katsnelson, K. S. Novoselov, D. Obergfell, S. Roth, C. Girit, and A. Zettl, "On the roughness of single- and bi-layer graphene membranes," SOLID STATE COMMUNICATIONS **143**, 101–109 (2007).
74. N. Dubrovinskaia, L. Dubrovinsky, F. Langenhorst, S. Jacobsen, and C. Liebske, "Nanocrystalline diamond synthesized from C60," DIAMOND AND RELATED MATERIALS **14**, 16–22 (2005).
75. I. Aharonovich, A. D. Greentree, and S. Prawer, "Diamond photonics," NATURE PHOTONICS **5**, 397–405 (2011).
76. C. J. H. Wort and R. S. Balmer, "Diamond as an electronic material," MATERIALS TODAY **11**, 22–28 (2008).

77. C. Artini, M. L. Muolo, and A. Passerone, "Diamond-metal interfaces in cutting tools: a review," JOURNAL OF MATERIALS SCIENCE **47**, 3252–3264 (2012).
78. J. R. Maze, P. L. Stanwix, J. S. Hodges, S. Hong, J. M. Taylor, P. Cappellaro, L. Jiang, M. V. G. Dutt, E. Togan, A. S. Zibrov, A. Yacoby, R. L. Walsworth, and M. D. Lukin, "Nanoscale magnetic sensing with an individual electronic spin in diamond," NATURE **455**, 644–U41 (2008).
79. B. Naydenov, V. Richter, J. Beck, M. Steiner, P. Neumann, G. Balasubramanian, J. Achard, F. Jelezko, J. Wrachtrup, and R. Kalish, "Enhanced generation of single optically active spins in diamond by ion implantation," APPLIED PHYSICS LETTERS **96**, 163108 (2010).
80. P. Neumann, J. Beck, M. Steiner, F. Rempp, H. Fedder, P. R. Hemmer, J. Wrachtrup, and F. Jelezko, "Single-Shot Readout of a Single Nuclear Spin," SCIENCE **329**, 542–544 (2010).
81. P. Neumann, R. Kolesov, B. Naydenov, J. Beck, F. Rempp, M. Steiner, V. Jacques, G. Balasubramanian, M. L. Markham, D. J. Twitchen, S. Pezzagna, J. Meijer, J. Twamley, F. Jelezko, and J. Wrachtrup, "Quantum register based on coupled electron spins in a room-temperature solid," NATURE PHYSICS **6**, 249–253 (2010).
82. V. V. Dobrovitski, G. D. Fuchs, A. L. Falk, C. Santori, and D. D. Awschalom, "Quantum Control Over Single Spins in Diamond," Annual Review of Condensed Matter Physics **4**, 23-50 (2013).
83. M. Woydt, "Oil Free Machinery and Zero Wear- Dream or Reality?," Tribology Online **6**, 101–112 (2011).
84. A. K. Geim and K. S. Novoselov, "The rise of graphene," NATURE MATERIALS **6**, 183–191 (2007).
85. J. Zang, S. Ryu, N. Pugno, Q. Wang, Q. Tu, M. J. Buehler, and X. Zhao, "Multifunctionality and control of the crumpling and unfolding of large-area graphene," Nat Mater online DOI 10.1038/nmat3542 (2013).
86. G. Mikheev, R. Zonov, A. Obraztsov, and Y. Svirko, "Giant optical rectification effect in nanocarbon films," APPLIED PHYSICS LETTERS **84**, 4854–4856 (2004).
87. G. M. Mikheev, R. G. Zonov, A. N. Obraztsov, and D. G. Kalyuzhny, "A device for testing a fast nanographite photodetector at high temperatures," INSTRUMENTS AND EXPERIMENTAL TECHNIQUES **51**, 456–461 (2008).
88. Y. Chen, F. Guo, A. Jachak, S.-P. Kim, D. Datta, J. Liu, I. Kulaots, C. Vaslet, H. D. Jang, J. Huang, A. Kane, V. B. Shenoy, and R. H. Hurt, "Aerosol Synthesis of Cargo-Filled Graphene Nanosacks," NANO LETTERS **12**, 1996–2002 (2012).
89. A. N. Obraztsov and V. I. Kleshch, "Cold and Laser Stimulated Electron Emission from Nanocarbons," Journal of Nanoelectronics and Optoelectronics **4**, 207–219 (2009).

90. S. Ghosh, W. Bao, D. L. Nika, S. Subrina, E. P. Pokatilov, C. N. Lau, and A. A. Balandin, "Dimensional crossover of thermal transport in few-layer graphene," NATURE MATERIALS **9**, 555–558 (2010).
91. J. Benedikt, "Plasma-chemical reactions: low pressure acetylene plasmas," JOURNAL OF PHYSICS D-APPLIED PHYSICS **43**, 043001 (2010).
92. G. Lombardi, K. Hassouni, G. Stancu, L. Mechold, J. Ropcke, and A. Gicquel, "Modeling of microwave discharges of H_2 admixed with CH_4 for diamond deposition," JOURNAL OF APPLIED PHYSICS **98**, 053303 (2005).
93. A. von Keudell, "Surface processes during thin-film growth," PLASMA SOURCES SCIENCE & TECHNOLOGY **9**, 455–467 (2000).
94. M. Ashfold, P. May, J. Petherbridge, K. Rosser, J. Smith, Y. Mankelevich, and N. Suetin, "Unravelling aspects of the gas phase chemistry involved in diamond chemical vapour deposition," PHYSICAL CHEMISTRY CHEMICAL PHYSICS **3**, 3471–3485 (2001).
95. P. W. May, M. N. R. Ashfold, and Y. A. Mankelevich, "Microcrystalline, nanocrystalline, and ultrananocrystalline diamond chemical vapor deposition: Experiment and modeling of the factors controlling growth rate, nucleation, and crystal size," JOURNAL OF APPLIED PHYSICS **101**, 053115 (2007).
96. P. W. May and Y. A. Mankelevich, "Experiment and modeling of the deposition of ultrananocrystalline diamond films using hot filament chemical vapor deposition and $Ar/CH_4/H_2$ gas mixtures: A generalized mechanism for ultrananocrystalline diamond growth," JOURNAL OF APPLIED PHYSICS **100**, 024301 (2006).
97. T. Farouk, B. Farouk, A. Gutsol, and A. Fridman, "Atmospheric pressure methane-hydrogen dc micro-glow discharge for thin film deposition," JOURNAL OF PHYSICS D-APPLIED PHYSICS **41**, 175202 (2008).
98. J. A. Stillahn, K. J. Trevino, and E. R. Fisher, "Plasma Diagnostics for Unraveling Process Chemistry," ANNUAL REVIEW OF ANALYTICAL CHEMISTRY **1**, 261–291 (2008).
99. H. WINTERS and J. COBURN, "SURFACE SCIENCE ASPECTS OF ETCHING REACTIONS," SURFACE SCIENCE REPORTS **14**, 161–269 (1992).
100. J. Zhou and E. R. Fisher, "Surface reactivity and energetics of CH radicals during plasma deposition of hydrogenated diamondlike carbon films," JOURNAL OF PHYSICAL CHEMISTRY B **110**, 21911–21919 (2006).
101. N. Bibinov, D. Kokh, N. Kolokolov, V. Kostenko, D. Meyer, I. Vinogradov, and K. Wiesemann, "A comparative study of the electron distribution function in the positive columns in N_2 and N_2/He dc glow discharges by optical spectroscopy and probes," PLASMA SOURCES SCIENCE & TECHNOLOGY **7**, 298–309 (1998).
102. F. Gordillo-Vazquez, M. Camero, and C. Gomez-Aleixandre, "Spectroscopic measurements of the electron temperature in low pressure radiofrequency

$Ar/H_2/C_2H_2$ and $Ar/H_2/CH_4$ plasmas used for the synthesis of nanocarbon structures," PLASMA SOURCES SCIENCE & TECHNOLOGY **15**, 42–51 (2006).
103. S. Lee, Z. Lin, and X. Jiang, "CVD diamond films: nucleation and growth," MATERIALS SCIENCE & ENGINEERING R-REPORTS **25**, 123–154 (1999).
104. C. Chu, M. Develyn, R. Hauge, and J. Margrave, "Mechanism of diamond growth by chemical vapor deposition on diamond (100), (111), and (110) surfaces – C_{13} studies," JOURNAL OF APPLIED PHYSICS **70**, 1695–1705 (1991).
105. H. Lange, "Spectral diagnostics of helium-carbon arc plasma during carbon nanostructure formation," FULLERENE SCIENCE AND TECHNOLOGY **5**, 1177–1201 (1997).
106. H. Lange, A. Huczko, and P. Byszewski, "Spectroscopic study of C-2 in carbon arc discharge," SPECTROSCOPY LETTERS **29**, 1215–1228 (1996).
107. H. Lange, K. Saidane, M. Razafinimanana, and A. Gleizes, "Temperatures and C 2 column densities in a carbon arc plasma," Journal of Physics D: Applied Physics **32**, 1024-1030 (1999).
108. P. Deak, A. Kovats, P. Csikvary, I. Maros, and G. Hars, "Ethynyl (C2H): A major player in the chemical vapor deposition of diamond," APPLIED PHYSICS LETTERS **90**, 051503 (2007).
109. M. Frenklach and H. Wang, "Detailed surface and gas-phase chemical-kinetics of diamond deposition," PHYSICAL REVIEW B **43**, 1520–1545 (1991).
110. K. Hassouni, F. Silva, and A. Gicquel, "Modelling of diamond deposition microwave cavity generated plasmas," JOURNAL OF PHYSICS D-APPLIED PHYSICS **43**, 153001 (2010).
111. J. Rabeau, P. John, J. Wilson, and Y. Fan, "The role of C-2 in nanocrystalline diamond growth," JOURNAL OF APPLIED PHYSICS **96**, 6724–6732 (2004).
112. P. Redfern, D. Horner, L. Curtiss, and D. Gruen, "Theoretical studies of growth of diamond (110) from dicarbon," JOURNAL OF PHYSICAL CHEMISTRY **100**, 11654–11663 (1996).
113. M. Sternberg, D. Horner, P. Redfern, P. Zapol, and L. Curtiss, "Theoretical studies of CN and C-2 addition to a (100)-(2x1) diamond surface: Nanocrystalline diamond growth mechanisms," JOURNAL OF COMPUTATIONAL AND THEORETICAL NANOSCIENCE **2**, 207–213 (2005).
114. K. Teii and T. Ikeda, "Effect of enhanced C-2 growth chemistry on nanodiamond film deposition," APPLIED PHYSICS LETTERS **90**, 111504 (2007).
115. A. Bogaerts, M. Eckert, M. Mao, and E. Neyts, "Computer modelling of the plasma chemistry and plasma-based growth mechanisms for nanostructured materials," JOURNAL OF PHYSICS D-APPLIED PHYSICS **44**, 174030 (2011).

116. P. Bachmann, D. Leers, and H. Lydtin, "Towards a general concept of diamond chemical vapor-deposition," DIAMOND AND RELATED MATERIALS **1**, 1–12 (1991).
117. V. Polushkin, A. Rakhimov, V. Samordov, N. Suetin, and M. Timofeyev, "OES study of plasma processes in DC discharge during diamond film deposition," DIAMOND AND RELATED MATERIALS **3**, 1385–1388 (1994).
118. Y. P. Raizer, *Gas Discharge Physics* (Springer-Verlag, 1991).
119. M. W. Kelly, J. C. Richley, C. M. Western, M. N. R. Ashfold, and Y. A. Mankelevich, "Exploring the Plasma Chemistry in Microwave Chemical Vapor Deposition of Diamond from C/H/O Gas Mixtures," JOURNAL OF PHYSICAL CHEMISTRY A **116**, 9431–9446 (2012).
120. J. Ma, J. C. Richley, M. N. R. Ashfold, and Y. A. Mankelevich, "Probing the plasma chemistry in a microwave reactor used for diamond chemical vapor deposition by cavity ring down spectroscopy," JOURNAL OF APPLIED PHYSICS **104**, 103305 (2008).
121. C. Rennick, J. Smith, M. Ashfold, and A. Orr-Ewing, "Cavity ring-down spectroscopy measurements of the concentrations of C-2(X1 Sigma(+)(g)) radicals in a DC arc jet reactor used for chemical vapour deposition of diamond films," CHEMICAL PHYSICS LETTERS **383**, 518–522 (2004).
122. J. Wills, J. Smith, W. Boxford, J. Elks, M. Ashfold, and A. Orr-Ewing, "Measurements of C-2 and CH concentrations and temperatures in a dc arc jet using cavity ring-down spectroscopy," JOURNAL OF APPLIED PHYSICS **92**, 4213–4222 (2002).
123. A. Goyette, J. Lawler, L. Anderson, D. Gruen, T. McCauley, D. Zhou, and A. Krauss, "C-2 swan band emission intensity as a function of C-2 density," PLASMA SOURCES SCIENCE & TECHNOLOGY **7**, 149–153 (1998).
124. P. John, J. Rabeau, and J. Wilson, "The cavity ring-down spectroscopy of C-2 in a microwave plasma," DIAMOND AND RELATED MATERIALS **11**, 608–611 (2002).
125. S. A. Lyashenko, A. P. Volkov, R. R. Ismagilov, and A. N. Obraztsov, "Field electron emission from nanodiamond," TECHNICAL PHYSICS LETTERS **35**, 249–252 (2009).
126. A. L. Chuvilin, V. L. Kuznetsov, and A. N. Obraztsov, "Chiral carbon nanoscrolls with a polygonal cross-section," CARBON **47**, 3099–3105 (2009).
127. K. A. Jenkins, "Graphene in High-Frequency Electronics This two-dimensional form of carbon has properties not seen in any other substance," AMERICAN SCIENTIST **100**, 388–397 (2012).
128. S. Bae, H. Kim, Y. Lee, X. Xu, J.-S. Park, Y. Zheng, J. Balakrishnan, T. Lei, H. R. Kim, Y. I. Song, Y.-J. Kim, K. S. Kim, B. Ozyilmaz, J.-H. Ahn, B. H. Hong, and S. Iijima, "Roll-to-roll production of 30-inch graphene films for transparent electrodes," NATURE NANOTECHNOLOGY **5**, 574–578 (2010).
129. Q. Yu, L. A. Jauregui, W. Wu, R. Colby, J. Tian, Z. Su, H. Cao, Z. Liu, D. Pandey, D. Wei, T. F. Chung, P. Peng, N. P. Guisinger, E. A. Stach, J. Bao, S.-

S. Pei, and Y. P. Chen, "Control and characterization of individual grains and grain boundaries in graphene grown by chemical vapour deposition," NATURE MATERIALS **10**, 443–449 (2011).

130. H. Wang, G. Wang, P. Bao, S. Yang, W. Zhu, X. Xie, and W.-J. Zhang, "Controllable Synthesis of Submillimeter Single-Crystal Monolayer Graphene Domains on Copper Foils by Suppressing Nucleation," JOURNAL OF THE AMERICAN CHEMICAL SOCIETY **134**, 3627–3630 (2012).
131. Y. A. Wu, Y. Fan, S. Speller, G. L. Creeth, J. T. Sadowski, K. He, A. W. Robertson, C. S. Allen, and J. H. Warner, "Large Single Crystals of Graphene on Melted Copper Using Chemical Vapor Deposition," ACS NANO **6**, 5010–5017 (2012).
132. L. Gao, W. Ren, H. Xu, L. Jin, Z. Wang, T. Ma, L.-P. Ma, Z. Zhang, Q. Fu, L.-M. Peng, X. Bao, and H.-M. Cheng, "Repeated growth and bubbling transfer of graphene with millimetre-size single-crystal grains using platinum," NATURE COMMUNICATIONS **3**, 699 (2012).
133. T. Iwasaki, H. J. Park, M. Konuma, D. S. Lee, J. H. Smet, and U. Starke, "Long-Range Ordered Single-Crystal Graphene on High-Quality Heteroepitaxial Ni Thin Films Grown on MgO(111)," NANO LETTERS **11**, 79–84 (2011).
134. L. M. Malard, M. A. Pimenta, G. Dresselhaus, and M. S. Dresselhaus, "Raman spectroscopy in graphene," PHYSICS REPORTS-REVIEW SECTION OF PHYSICS LETTERS **473**, 51–87 (2009).
135. M. A. Pimenta, G. Dresselhaus, M. S. Dresselhaus, L. G. Cancado, A. Jorio, and R. Saito, "Studying disorder in graphite-based systems by Raman spectroscopy," Physical chemistry chemical physics **9**, 1276–1290 (2007).
136. J. S. Bunch, S. S. Verbridge, J. S. Alden, A. M. van der Zande, J. M. Parpia, H. G. Craighead, and P. L. McEuen, "Impermeable atomic membranes from graphene sheets," NANO LETTERS **8**, 2458–2462 (2008).
137. T. Hantschel, P. Niedermann, T. Trenkler, and W. Vandervorst, "Highly conductive diamond probes for scanning spreading resistance microscopy," APPLIED PHYSICS LETTERS **76**, 1603–1605 (2000).
138. M. Jarvis, R. Perez, and M. Payne, "Can atomic force microscopy achieve atomic resolution in contact mode?," PHYSICAL REVIEW LETTERS **86**, 1287–1290 (2001).
139. B. Bhushan and V. Koinkar, "Nanoindentation hardness measurements using atomic-force microscopy," APPLIED PHYSICS LETTERS **64**, 1653–1655 (1994).
140. J. Bae, T. Ono, and M. Esashi, "Scanning probe with an integrated diamond heater element for nanolithography," APPLIED PHYSICS LETTERS **82**, 814–816 (2003).

141. K. Kim, N. Moldovan, C. Ke, H. Espinosa, X. Xiao, J. Carlisle, and O. Auciello, "Novel ultrananocrystalline diamond probes for high-resolution low-wear nanolithographic techniques," SMALL **1**, 866–874 (2005).
142. P. Maletinsky, S. Hong, M. S. Grinolds, B. Hausmann, M. D. Lukin, R. L. Walsworth, M. Loncar, and A. Yacoby, "A robust scanning diamond sensor for nanoscale imaging with single nitrogen-vacancy centres," NATURE NANOTECHNOLOGY **7**, 320–324 (2012).
143. B. Mesa and S. Magonov, "Novel diamond/sapphire probes for scanning probe microscopy applications," JOURNAL OF PHYSICS: CONFERENCE SERIES **61**, 770 (2007).
144. F. Baik, Y. Baik, and D. Jeon, "Diamond tip fabrication by air-plasma etching of diamond with an oxide mask," DIAMOND AND RELATED MATERIALS **8**, 2169–2171 (1999).
145. H. Uetsuka, T. Yamada, and S. Shikata, "ICP etching of polycrystalline diamonds: Fabrication of diamond nano-tips for AFM cantilevers," DIAMOND AND RELATED MATERIALS **17**, 728–731 (2008).
146. Q. Wang, J. J. Li, A. Z. Jin, Z. L. Wang, P. Xu, and C. Z. Gu, "The growth and characterization of diamond cone arrays formed by plasma etching," DIAMOND AND RELATED MATERIALS **15**, 866–869 (2006).
147. D. Alvarez, M. Fouchier, J. Kretz, J. Hartwich, S. Schoemann, and W. Vandervorst, "Fabrication and characterization of full diamond tips for scanning spreading-resistance microscopy," MICROELECTRONIC ENGINEERING **73-4**, 910–915 (2004).
148. P. Niedermann, W. Hanni, D. Morel, A. Perret, N. Skinner, P. Indermuhle, N. de Rooij, and P. Buffat, "CVD diamond probes for nanotechnology," APPLIED PHYSICS A-MATERIALS SCIENCE & PROCESSING **66**, S31–S34 (1998).
149. R. Agrawal, N. Moldovan, and H. D. Espinosa, "An energy-based model to predict wear in nanocrystalline diamond atomic force microscopy tips," JOURNAL OF APPLIED PHYSICS **106**, 064311 (2009).
150. van der Drift A, "Evolutionary selection, a principle governing growth orientation in vapour-deposited layers," Philips Research Report **22**, 267–288 (1967).
151. S. Osswald, M. Havel, V. Mochalin, G. Yushin, and Y. Gogotsi, "Increase of nanodiamond crystal size by selective oxidation," DIAMOND AND RELATED MATERIALS **17**, 1122–1126 (2008).
152. S. Lee, H. Peng, X. Zhou, N. Wang, C. Lee, I. Bello, and Y. Lifshitz, "A nucleation site and mechanism leading to epitaxial growth of diamond films," SCIENCE **287**, 104–106 (2000).
153. C. Y. Zhang, C. X. Wang, Y. H. Yang, and G. W. Yang, "A Nanoscaled Thermodynamic Approach in Nucleation of CVD Diamond on Nondiamond Surfaces," The Journal of Physical Chemistry B **108**, 2589–2593 (2004).

Rinat Ismagilov

Formation of carbon nano- and micro-structures by chemical vapor deposition

Carbon is material of great importance for the mankind. In its elementary form carbon provides a basis for organic life, while the allotropes of condensed state carbon gave birth to a number of technical applications. In this thesis formation of solid state carbon films with advanced properties via condensation of atoms from plasma activated carbonaceous environment is considered. The researches were conducted on Production and Characterization of the carbon films, including development of the plasma assisted chemical vapor deposition, Raman spectroscopy, scanning and transmission electron microscopies, electron diffraction, optical emission spectroscopy. Prospective applicability of the carbon films is also considered.

UNIVERSITY OF
EASTERN FINLAND

Publications of the University of Eastern Finland
Dissertations in Forestry and Natural Sciences

ISBN: 978-952-61-1264-0 (nid.)
ISBN: 978-952-61-1265-7 (PDF)
ISSNL: 1798-5668
ISSN: 1798-5668
ISSN: 1798-5676 (PDF)